Neural coding of distinct motor patterns during *Drosophila* courtship song

Hiroshi M. Shiozaki[1,*], Kaiyu Wang[1,3], Joshua L. Lillvis[1], Min Xu[1], Barry J. Dickson[1,2] & David L. Stern[1,*]

[1]Janelia Research Campus, Howard Hughes Medical Institute, Ashburn, VA, USA.

[2]Queensland Brain Institute, University of Queensland, St Lucia, QLD, Australia.

[3]Present address: Institute of Neuroscience, Lingang Laboratory, Shanghai Center for Brain Science and Brain-Inspired Intelligence Technology, Shanghai, China.

*Correspondence: shiozaki.h@gmail.com (H.M.S.), sternd@janelia.hhmi.org (D.L.S.)

Abstract

Animals flexibly switch between different actions by changing neural activity patterns for motor control. Courting *Drosophila melanogaster* males produce two different acoustic signals, pulse and sine song, each of which can be promoted by artificial activation of distinct neurons. However, how the activity of these neurons implements flexible song production is unknown. Here, we developed an assay to record neuronal calcium signals in the ventral nerve cord, which contains the song motor circuit, in singing flies. We found that sine-promoting neurons, but not pulse-promoting neurons, show strong activation during sine song. In contrast, both pulse- and sine-promoting neurons are active during pulse song. Furthermore, population calcium imaging in the song circuit suggests that sine song involves activation of a subset of neurons that are also active during pulse song. Thus, differential activation of overlapping, rather than distinct, neural populations underlies flexible motor actions during acoustic communication in *D. melanogaster*.

Introduction

Animals flexibly switch between different movements to adapt to a changing environment. A common mechanism to produce diverse movements is to activate separate neural populations, each dedicated to one movement. For example, during locomotion, flexor and extensor muscles in the vertebrate limb alternately contract through activation of different neural populations in the spinal cord[1, 2]. This type of motor control often underlies movements that involve contractions of distinct populations of muscles. Diverse movements can also be produced by differentially contracting overlapping sets of muscles, but little is known about how these movements are controlled by the motor system. These movements could arise through activation of separate neural populations, as in the movements controlled by distinct muscles, or by activation of overlapping neural populations.

During courtship, *Drosophila* males vibrate their wings in specific patterns to produce acoustic communication signals called courtship song. Each species produces unique courtship songs[3-5], and these signals can be used by females to bias their mate choice[6, 7]. In *Drosophila melanogaster*, the courtship song is composed of two primary types of song, pulse and sine. Pulse song comprises a series of sound impulses separated by short inter-pulse intervals[8], whereas sine song is a continuous, sinusoidal sound (Fig. 1a). These two types of song influence females' receptivity to males in different ways[9, 10], and males dynamically switch between pulse and sine song depending on sensory feedback from females[6] as well as based on internal states[11]. The wing movements that produce these sounds are shaped by wing control muscles[12], which induce rapid changes in wing motion through coordinated firing[13]. Most of the control muscles are active during pulse song production, whereas a subset of these active muscles becomes silent during sine song production[13, 14]. Thus, the two song patterns are produced by recruiting overlapping, rather than distinct, sets of wing control muscles.

The song motor circuit resides in the ventral nerve cord (VNC). Wing motor neurons extend dendrites into the VNC[12, 14-16] where they receive input from thoracic interneurons that, in turn, integrate song promoting descending commands from the brain[3, 8, 11, 17-21]. Activity of thoracic interneurons is sufficient to generate song, since activation of certain neurons in decapitated males can drive patterned song[3, 22]. In the VNC, neurons that express the sex determination genes *fruitless* (*fru*) and/or *doublesex* (*dsx*) are thought to form neural circuits for song production[21, 23, 24]. Some of these neurons appear to contribute differentially to pulse and sine song. For example, silencing the activity of dPR1 neurons impairs pulse song production[21], whereas silencing TN1A neurons reduces sine but not pulse song production[23]. However, it remains unclear whether and how the activity of these neurons implements flexible production of pulse and sine song because no existing preparation allows the recording of neural activity in the VNC during singing.

Here, we developed a two-photon calcium imaging assay for recording signals from neurons in the song motor circuits while flies sang alternate bouts of pulse and sine song. We found that dPR1 neurons are selectively active during pulse, whereas TN1A neurons are active during both pulse and sine song. Furthermore, pan-neuronal calcium imaging of the wing-related neuropils in the VNC suggests that sine song involves activation of a subset of neurons that are active during pulse song. Thus, the neural circuit for sine song is largely nested within the circuit for pulse song. Together, our results show that activation of overlapping, rather than distinct, populations of neurons in the central

motor circuit underlie flexible production of different types of acoustic communication signals in *D. melanogaster*.

Results

Activation of dPR1 and TN1A neurons differently modulates song production. To study how pulse and sine song are produced, we built driver lines for dPR1 and TN1A using the split-Gal4 method[25, 26]. Both dPR1 and TN1A neurons express the sex determination gene *dsx*[21, 23]. The dPR1 driver line cleanly labels a pair of VNC neurons (Fig. 1b and Extended Data Fig. 1a,b) whose cell body locations and innervation patterns match those of dPR1[21]. As expected, these labeled neurons express *dsx* (Extended Data Fig. 1c). The driver line for TN1A was constructed using *dsx*-DBD as a hemidriver and thus labels a subset of *dsx*-expressing neurons. This line labels approximately four VNC neurons per hemisphere whose morphology matches that of TN1A[23] (Fig. 1b and Extended Data Fig. 1a,d,e).

dPR1 and TN1A were previously implicated in pulse and sine song production, respectively[18, 21, 23]. However, due to limitations in available reagents, it has remained unclear how specifically these neurons contribute to each song type. To address this issue, we expressed the light-gated cation channel CsChrimson[27] in dPR1 or TN1A neurons and applied activation light in solitary males placed in song recording chambers (Extended Data Fig. 1f). Optogenetic activation of dPR1 acutely elicited pulse but not sine song over a range of stimulation, whereas activation of TN1A induced sine but not pulse song (Extended Data Fig. 1g–o). Thus, dPR1 and TN1A are capable of inducing pulse and sine song, respectively.

We next examined the activation effects of dPR1 and TN1A in the context of natural courtship. Male flies were paired with virgin females to induce song. We applied optogenetic activation light to test how dPR1 and TN1A activation affected ongoing song production (Fig. 1c). To avoid excessive perturbations of the song system, we used light intensities that induced song only moderately when applied in solitary flies (Extended Data Fig. 1i,l). Moderate dPR1 activation (11.9 uW/mm^2) increased pulse song while reducing sine song throughout the stimulation period (Fig. 1d–f and Extended Data Fig. 2a,b). Furthermore, weak dPR1 activation (4.0 uW/mm^2) suppressed sine song without promoting pulse song (Fig. 1d–f). In contrast, TN1A activation promoted sine song throughout the stimulation period but reduced pulse song only at the stimulation onset (Fig. 1g–i and Extended Data Fig. 2a,c). These results suggest that while activation of dPR1 and TN1A promote song production of their preferred type, only dPR1 activation can persistently suppress production of the non-preferred song type.

Changes in the amounts of pulse and sine song can be caused by factors such as changes in the probability of song initiation, song termination, and song type switching. Indeed, all of these probabilities were modulated by dPR1 and TN1A activation (Extended Data Fig. 2d–f). Notably, the effects of dPR1 and TN1A activation were qualitatively different from each other. For example, dPR1 activation increased the probability of initiating pulse song but not sine song, while TN1A activation increased the initiation probabilities of both pulse and sine song (Extended Data. Fig. 2d). Optogenetically induced changes in the amount of song sometimes reflected countervailing effects of multiple parameters. For example, TN1A activation promoted pulse song by increasing pulse initiation probability and decreasing pulse termination probability, while at the same time reducing pulse by increasing the probability of pulse to sine transitions (Extended Data Fig. 2d–f). These counteracting effects resulted in no change in the pulse amount from

91 the pre-stimulation period to the later part of the stimulation period (Fig. 1g–i). Taken together, activation of dPR1and
92 TN1A differently altered pulse and sine song production by modulating multiple aspects of singing behavior.
93
94 **dPR1 and TN1A neurons exhibit different activity patterns during song.** We next examined the activity of dPR1
95 and TN1A neurons during pulse and sine song. There has been no preparation that allows recording the activity of VNC
96 neurons in singing flies. This partly stems from two technical challenges. First, wing vibration is dependent on muscle-
97 induced oscillatory movements of the thorax[28] and thus attaching the thorax, which houses the VNC, to the recording
98 apparatus often disturbs these oscillations. Second, wing muscles are adjacent to the VNC and are easily damaged
99 during dissection required to image the VNC. To overcome these challenges, we glued parts of the legs, instead of the
100 thorax, to the recording plate and dissected the ventral side of the thorax where wing muscles are absent (Fig. 2a). This
101 novel assay provides optical access to VNC neurons while allowing approximately normal wing vibrations for song.
102 Song was induced by optogenetic activation of neurons labeled by a LexA line (R22D03-LexA) that we term the
103 "song driver" (Fig. 2b). This driver line labels multiple neurons including the male specific brain neurons P1, which
104 integrate multisensory cues and promote the initiation and persistence of courtship behavior[17, 19, 21, 29-33] (Extended Data
105 Fig. 3a). Optogenetic activation of the neurons labeled by the song driver in tethered males induced alternating bouts of
106 pulse and sine song, even though the activation light was maintained at constant power (Fig. 2c and Extended Data Fig.
107 3b,c). The bout durations of the induced pulse and sine song were similar to those produced during normal courtship in
108 freely moving flies (Extended Data Fig. 3d). Removal of the head eliminated the production of song during optogenetic
109 stimulation (Extended Data Fig. 3b,e). This effect was not caused by decapitation-induced physical damage because
110 optogenetic activation of pIP10, the song promoting descending neuron[3, 8, 11, 17-21], in the same preparation elicited song
111 in decapitated flies (Extended Data Fig. 3f,g). These results indicate that neurons in the brain, but not in the VNC, are
112 required for inducing song by optogenetic stimulation of the song driver.
113 To characterize the activity of dPR1 and TN1A during pulse and sine song, we performed two-photon imaging of
114 the genetically encoded calcium indicator jGCaMP7f[34] expressed in dPR1 or TN1A neurons with the split-Gal4 lines
115 while inducing song by optogenetic stimulation with the song driver. By imaging the cell bodies, we extracted the
116 calcium signals of individual neurons. Optogenetic stimulation induced an acute increase in calcium signals of dPR1
117 neurons (Fig. 2d–f, Extended Data Fig. 4a,b and Supplementary Video 1). Consistent with a role of dPR1 in song
118 production, both dPR1 calcium signals and the amount of song scaled with the strength of optogenetic stimulation of
119 the song driver on average (Extended Data Fig. 4c,d). We then examined the calcium signals of individual trials and
120 found that the dPR1 calcium signals repeatedly increased and decreased over the course of constant optogenetic
121 stimulation (Fig. 2e). Notably, the timing of calcium signal modulation aligned with that of song type transitions. The
122 calcium signal increased during transitions from sine to pulse and decreased during transitions from pulse to sine (Fig.
123 2e,g,h). The preference for pulse is consistent with the observation that optogenetic activation of dPR1 promotes pulse
124 song (Fig. 1).
125 Calcium dynamics measured at the soma are known to be slower than those at the neuropil[35]. Indeed, dPR1 signals
126 measured at the neuropil showed more rapid modulation than somatic signals (Extended Data Fig. 4e–g). The decay

127 rate of the neuropil signal during sine song (Extended Data Fig. 4e) was comparable to the decay kinetics of jGCaMP7f
128 after high frequency firing[34]. These results suggest that dPR1 neurons are active during pulse song but not during sine
129 song.
130 As we observed for dPR1, calcium signals of individual TN1A neurons increased in response to optogenetic
131 stimulation of the song driver (Fig. 2i,j, Extended Data Fig. 4h,i, and Supplementary Video 2). As expected for a role of
132 TN1A in song production, both TN1A calcium signals and the amount of song increased with the stimulation strength
133 on average (Extended Data Fig. 4j,k). We then analyzed data in individual trials and found that TN1A calcium signals
134 increased when the song type switched from pulse to sine (Fig. 2i,k,l), consistent with the observation that optogenetic
135 activation of TN1A promotes sine (Fig. 1). However, TN1A calcium signals did not decrease but remained unchanged
136 when the song type switched from sine to pulse (Fig. 2i,k,l). This pattern contrasts with the dPR1 calcium signals,
137 which rapidly decreased after the transition to the non-preferred song type (Fig. 2g). The different calcium signal
138 patterns between dPR1 and TN1A did not result from slower kinetics of calcium at the cell body than in the neuropil,
139 because TN1A calcium signals measured at the neuropil decreased only slightly, if at all, when the song type switched
140 from sine to pulse (Extended Data Fig. 4l–n). These results suggest that TN1A neurons are active during both pulse and
141 sine song with a preference for sine.
142 The tethered flies occasionally produced pulse song outside of the optogenetic stimulation periods, as observed
143 during intermittent stimulation of P1 neurons in freely moving isolated male flies[17, 19]. We observed an increase in
144 calcium signals in both dPR1 and TN1A when flies sang pulse outside of the optogenetic stimulation periods (Extended
145 Data Fig. 4o,p). This result further supports the conclusion that pulse song involves activation of both dPR1 and TN1A.
146 As an independent test of pulse-related activity, we recorded calcium signals from dPR1 and TN1A while pulse
147 song was induced by activating pIP10, a pair of song promoting descending neurons[3, 8, 11, 17-21]. We expressed
148 CsChrimson in pIP10 using a new split-LexA line (Extended Data Fig. 5a,b) while driving the expression of jGCaMP7s
149 in dPR1 or TN1A. Optogenetic activation with the split-LexA line induced predominantly pulse song in freely walking
150 flies (Extended Data Fig. 5c–f) as well as during calcium imaging (Extended Data Fig. 5h,j). Both dPR1 and TN1A
151 showed increased calcium signals when flies sang pulse song (Extended Data Fig. 5g–p). Thus, both the pulse-
152 promoting neurons dPR1 and the sine-promoting neurons TN1A are active during pulse song.
153
154 **Pulse- and sine-preferring TN1 neurons exhibit different activity patterns during song.** To examine whether the
155 different song-related activity patterns observed in dPR1 and TN1A are a general property of pulse- and sine-preferring
156 neurons in the VNC, we focused on TN1 neurons. These neurons are male-specific, *dsx*-expressing VNC neurons
157 involved in song production[20, 23, 36]. There are approximately twenty-two TN1 neurons in each hemisphere[36], which are
158 composed of at least five anatomically defined cell types including TN1A[23] (Fig. 3a). While manipulation of the
159 activity of TN1 neurons primarily influences sine song production, a subset of TN1 neurons influences pulse song
160 production[20, 23].
161 To characterize the song-related activity of TN1 neurons, we recorded calcium signals from a large fraction of
162 individual TN1 neurons in each fly (Fig. 3a,b) while inducing song by optogenetic stimulation of the song driver. The

163 optogenetic stimulation elicited significant changes in calcium signals ($p < 0.05$, t-test, see Methods for detail) in
164 69.1% of the recorded TN1 neurons (56/89 neurons in 4 flies). For each neuron with significant responses, we
165 quantified the selectivity for song type with an index we termed the song-type preference (Fig. 3c and Extended Data
166 Fig., 6a,b). Most TN1 neurons showed significant preference for pulse or sine song (38/56 neurons in 4 flies; $p < 0.05$,
167 permutation test), with most preferring sine song (n = 25/38 neurons in 4 flies) (Fig. 3c). The average number of sine-
168 preferring neurons in each fly (n = 6.3 neurons per hemisphere) is larger than the number of neurons labeled by the
169 TN1A split-Gal4 driver (n = 4 neurons per hemisphere), suggesting that the sine-preferring population includes neurons
170 that were not labeled with the TN1A split-Gal4 line.
171 As observed for dPR1 and TN1A, pulse- and sine-preferring TN1 neurons displayed increased calcium signals
172 during optogenetic stimulation of the song driver (Fig. 3d). Consistent with a role in song production, both populations
173 showed larger responses to stronger stimulation, during which more song was produced (Extended Data Fig. 6c,d). To
174 examine the pulse- and sine-related activity, we calculated the average calcium signals during song-type transitions for
175 each population. We found that both populations showed increased calcium signals when the song switched to the
176 preferred type (Fig. 3e–h). However, pulse- but not sine-preferring neurons showed decreased calcium signals when the
177 song switched to the non-preferred type (Fig. 3e–h). This result suggests that—as we observed for dPR1 and TN1A
178 neurons—both pulse- and sine-preferring TN1 neurons are active during pulse song, while only the sine-preferring
179 neurons show high activity levels during sine song.
180 To further characterize pulse-related activity in TN1 neurons, we drove pulse song by optogenetically activating
181 pIP10 while recording calcium signals from TN1 neurons. Optogenetic stimulation of pIP10 induced changes in
182 calcium signals in a large fraction of TN1 neurons (77/83 neurons in 4 flies; $p < 0.05$, t-test, see Methods for detail), of
183 which virtually all neurons displayed increased calcium signals when the flies produced pulse song (76/77 neurons;
184 Extended Data Fig. 6e–j). This result further supports the idea that pulse song involves the coactivation of pulse-
185 preferring and sine-preferring TN1 neurons during pulse song.
186
187 **Sine song involves activation of a subset of VNC neurons active during pulse song.** Optogenetic activation of dPR1
188 and TN1A neurons induces pulse and sine song, respectively (Fig. 1). This indicates that dPR1 and TN1A activation
189 drives different activity patterns in the song motor circuit. To characterize these activity patterns, we expressed
190 jGCaMP7s with a pan-neuronal driver and recorded calcium signals in the wing-related neuropils (Fig. 4a)[37], which are
191 innervated by at least tens of cell types[14, 16, 21, 23, 24, 31, 38], while optogenetically activating either dPR1 or TN1A (Fig.
192 4b). Since two-photon microscopy cannot resolve individual neuronal processes within dense projections, the measured
193 calcium signal in each voxel likely reflected the combined activity of multiple neurons. Activation of either cell type
194 led to widespread responses in the imaged volume with overlapping, yet distinct spatial patterns (Fig. 4c and Extended
195 Data Fig. 7a,b). For example, dPR1 activation induced strong responses along the anterior-posterior axis around the
196 midline in the wing tectulum, whereas such responses were absent during TN1A activation ("Response in Dorsal" in
197 Fig. 4c and Extended Data Fig. 7a,b). These differential response patterns were not explained by calcium signals of the
198 neurons under optogenetic stimulation because dPR1 and TN1A neurons innervate highly overlapping regions

(Extended Data Fig. 7c,d). Thus, dPR1 and TN1A drive spatially different activity patterns in the wing-related neuropils.

These observations lead to the prediction that neurons responsive to dPR1 activation should be more active during pulse than sine song because dPR1 is selectively active during pulse song. By contrast, regions that responded specifically to TN1A activation should not show strong song-type-related activity modulation because TN1A is active during both pulse and sine song.

To test these predictions, we performed pan-neuronal volumetric calcium imaging in the wing-related neuropils with jGCaMP7f while inducing song with optogenetic activation of the song driver (Fig. 4d). Optogenetic stimulation elicited an increase in calcium signals in a large proportion of the recorded volume (Fig. 4e and Supplementary Video 3). We found that a subset of the activated voxels, including the ones around the midline in the wing tectulum, modulated calcium signals when the fly switched between pulse and sine song (Fig. 4e and Supplementary Videos 3 and 4). Notably, most of these song-type selective voxels showed decreased signals when the fly switched from pulse to sine song and increased signals when the song was switched from sine to pulse (Fig. 4e–h and Extended Data Fig. 8a–d). These observations suggest that sine song mostly involves activation of a subset of neurons that are active during pulse song.

When the fly sang pulse song outside the optogenetic stimulation periods, activation was observed in the voxels that showed stronger signals during pulse song and in voxels that did not show selectivity for song type (Extended Data Fig. 8e–h). This supports the idea that some neurons are similarly active during pulse and sine song.

The pulse-selective neural population is composed mainly of *fru*-expressing neurons. During pan-neuronal imaging, the voxels with stronger calcium signals during pulse than sine song were localized to a region called the mesothoracic triangle in the medial VNC[24] and the medial and lateral parts of the dorsal VNC (Fig. 4g,h). This distribution is similar to the innervation pattern of neurons expressing *fruitless* (*fru*)[21, 24] (Fig. 5a,b), a sex determination gene that regulates sexually dimorphic behaviors including courtship[39]. There are approximately 500 *fru*-expressing neurons in the male VNC, comprising at least 35 morphologically distinct cell types[21, 24]. Among these neurons, at least eight *fru* cell types, including dPR1, are known to innervate a VNC region overlapping the pulse-preferring voxels[21, 24].

To characterize overall activity of *fru* neurons, we expressed jGCaMP7f using *fru*-Gal4[40] and recorded calcium signals in the wing-related neuropils while inducing song by optogenetic activation of the song driver (Fig. 5a). We found that a large fraction of the voxels showed increased calcium signals during song (Fig. 5c). A subset of these activated voxels modulated calcium signals depending on song type, most of which showed stronger signals during pulse than sine song (Fig. 5c–e and Extended Data Fig. 9a–d). Voxels that did not show selectivity for song type were activated during pulse song produced outside the optogenetic stimulation periods (Extended Data Fig. 8e,f), suggesting that some of the *fru* neurons are similarly active during pulse and sine song. These results suggest that a group of *fru*-expressing neurons are activated during pulse song, whereas a subset of these activated neurons become silent during sine song.

The locations of the voxels with stronger signals during pulse than sine song (Fig. 5d,e) matched those detected

with pan-neuronal imaging (Fig. 4f,g), suggesting that *fru*-expressing neurons contribute to the song-type-selective signals observed during pan-neuronal imaging. To test this prediction, we took an intersectional genetic approach to express GCaMP in all non-*fru* neurons. We used a pan-neuronal driver to express Gal4, which drove the expression of jGCaMP7f, while suppressing jGCaMP7f expression in *fru* neurons with Gal80[24] (Fig. 5f). A large proportion of the imaged areas became activated during pulse and sine song (Fig. 5g), as in the pan-neuronal imaging (Fig. 4f). This indicates that song production involves activation of non-*fru* neurons. We then analyzed the changes in calcium signals between pulse and sine song and found a profound reduction in song-type-related signal modulation when jGCaMP7f expression was suppressed in *fru* neurons (Fig. 5g–i and Extended Data Fig. 9g,h). Notably, *fru* neurons comprise only a few percent of the neurons in the VNC[24, 41], indicating that these neurons have a disproportional impact on the song-type selective signal. Thus, the neural population that is active during pulse but not sine song is composed mainly of *fru*-expressing neurons (Fig. 5j).

Discussion

Previous studies have identified VNC neurons relevant for song production in *Drosophila melanogaster* by anatomical and activity manipulation approaches[3, 8, 11, 14, 16, 18, 20, 21, 23, 24]. Here, we developed a novel calcium imaging paradigm and characterized the activity of these neurons during singing. This physiological analysis revealed that the song motor system produces different types of song by differentially activating overlapping, rather than distinct, populations of neurons.

Optogenetic activation of dPR1 and TN1A neurons promoted pulse and sine song, respectively (Fig. 1). As expected from this phenotype, TN1A, but not dPR1, neurons showed strong activation during sine song (Fig. 2). In contrast, both dPR1 and TN1A were active during pulse song (Fig. 2). Consistent with this observation, sine song involved activation of a subset neurons that were also active during pulse song among TN1 neurons (Fig. 3). The same pattern was observed in pan-neuronal imaging of the wing-related neuropils (Fig. 4). The pan-neuronal imaging further suggests that pulse-preferring neurons outnumber sine-preferring neurons (Fig. 4). Together, our results suggest that pulse and sine song is produced by activating overlapping, rather than separate, populations of neurons in the song motor system. More specifically, a neural population active during both sine and pulse song underlies sine song, whereas additional neurons are recruited during pulse song. This activity pattern of VNC neurons mirrors that of wing muscles, many of which are activated during both song types and a few of which are active specifically during pulse[13, 14, 28]. Thus, the overlapping muscle activation patterns for pulse and sine song, first observed over 40 years ago, appear to be mirrored within the central circuits in the VNC.

A subset of TN1 neurons, including TN1A, are active during both pulse and sine, but showed higher activity during sine (Figs. 2 and 3). A population of wing control muscles show the same activity pattern as in these TN1 neurons[13], suggesting that the activity of these muscles is shaped by the dynamics of the sine-preferring neurons in the VNC. The muscles active during both song types have been proposed to control features of wing movement relevant for both pulse and sine song, such as the angle of attack[13, 14]. Indeed, silencing wing motor neurons necessary for normal production of sine song also affects pulse song production[14]. Thus, pulse and sine song involve activation of a shared

population of VNC neurons and muscles that might generate wing oscillation common to both song types.

dPR1 and a subset of TN1 neurons showed strong activation only during pulse song (Figs. 2 and 3). A group of wing control muscles are active during pulse but not sine song[13], suggesting that these muscles are controlled by dPR1 and similarly active neurons. These muscles are thought to contribute to the damping of wing oscillation during inter-pulse intervals as well as the initiation of wing movement at the end of each inter-pulse interval[13, 14]. Taken together, a group of muscles may generate wing oscillations during both pulse and sine while additional muscles are recruited during pulse song to shape inter-pulse intervals. This recruitment model provides a possible first order explanation for why neurons that prefer pulse song are more abundant than those that prefer sine song in the song motor system (Fig. 4). However, the transformation from muscle activity to song is likely to be more complex than this proposal. Silencing motor neurons that innervate certain wing control muscles induces changes in multiple aspects of song such as carrier frequencies and inter-pulse intervals, whereas silencing others has more specific effects[14, 16]. Furthermore, proprioceptive feedback also plays a role in shaping the timing of muscle activation[42]. Future work should address how activity of each neuron type in the central song circuit influences individual song parameters.

Pan-neuronal imaging showed that the activity of a population of neurons is stronger during pulse than sine song (Fig. 4). This population is predominantly composed of neurons expressing *fru* (Fig. 5). This result complements previous findings that *fru*-expressing neurons in the VNC are causally involved in pulse song production[21, 22]. Although we mainly analyzed the population activity in relation to song type, individual neurons may encode more specific features of pulse song such as the inter-pulse intervals. Indeed, manipulating the activity of different *fru*-expressing neuron types affects different pulse song parameters[21]. Furthermore, the VNC song circuit is capable of modulating the amplitude of pulse song depending on the distance to females[18]. Thus, the neural circuit for pulse song may be composed of subnetworks that control specific features of pulse song.

Courting males rapidly switch between pulse and sine song based on the behavioral context[6]. We found that the activity of pulse-preferring neurons, including dPR1, tracks ongoing song type, suggesting that these neurons play a key role in the context-dependent song selection. The descending neuron pIP10 provides song drive without specifying song type[3]. Thus, other neurons are likely to provide context information to the pulse-preferring neurons. Two possible sources of such input are the locomotor and the visual system, because *D. melanogaster* males produce pulse more frequently when they are distant from females and walking rapidly[6].

Production of diverse movements by overlapping neural populations is not unique to the *Drosophila* song system. For example, in the mammalian respiratory system, a group of neurons are active during fictive normal breathing, whereas a subset of these active neurons become inactive during fictive gasping[43]. Notably, normal breathing and gasping are likely to involve overlapping sets of muscles[44], similar to the production of pulse and sine songs[13, 28]. In contrast, movements that are driven by different sets of muscles, as in the case of alternating movements of left and right limbs during locomotion[2], may be controlled through separate neural populations. Thus, the pattern of muscle recruitment required for distinct movements may bias evolution toward either independent or overlapping neural circuit control of muscles.

In summary, we uncovered neural dynamics by which the motor system produces distinct types of courtship song in

307 *D. melanogaster*. Our novel functional imaging assay in behaving animals together with additional cell type specific
308 drivers for neurons in the song circuits[3, 14, 21, 23] provides a unique opportunity to investigate the circuit mechanisms of
309 neural computations underlying action selection and motor pattern generation.

310 **References**

311 1. Chalif, J.I., de Lourdes Martínez-Silva, M., Pagiazitis, J.G., Murray, A.J. & Mentis, G.Z. Control of mammalian locomotion
312 by ventral spinocerebellar tract neurons. *Cell* **185**, 328-344. e326 (2022).
313 2. Grillner, S. & El Manira, A. Current Principles of Motor Control, with Special Reference to Vertebrate Locomotion. *Physiol*
314 *Rev* **100**, 271-320 (2020).
315 3. Ding, Y.*, et al.* Neural Evolution of Context-Dependent Fly Song. *Curr Biol* **29**, 1089-1099.e1087 (2019).
316 4. Riabinina, O., Dai, M., Duke, T. & Albert, J.T. Active process mediates species-specific tuning of Drosophila ears. *Curr*
317 *Biol* **21**, 658-664 (2011).
318 5. Spieth, H.T. Courtship behavior in Drosophila. *Annu Rev Entomol* **19**, 385-405 (1974).
319 6. Coen, P.*, et al.* Dynamic sensory cues shape song structure in Drosophila. *Nature* **507**, 233-237 (2014).
320 7. Ritchie, M.G., Halsey, E.J. & Gleason, J.M. Drosophila song as a species-specific mating signal and the behavioural
321 importance of Kyriacou & Hall cycles in D. melanogaster song. *Anim Behav* **58**, 649-657 (1999).
322 8. Clemens, J.*, et al.* Discovery of a New Song Mode in Drosophila Reveals Hidden Structure in the Sensory and Neural
323 Drivers of Behavior. *Curr Biol* **28**, 2400-2412.e2406 (2018).
324 9. Bennet-Clark, H. & Ewing, A. Stimuli provided by courtship of male Drosophila melanogaster. *Nature* **215**, 669-671 (1967).
325 10. von Schilcher, F. The function of pulse song and sine song in the courtship of Drosophila melanogaster. *Animal Behaviour*
326 **24**, 622-625 (1976).
327 11. Calhoun, A.J., Pillow, J.W. & Murthy, M. Unsupervised identification of the internal states that shape natural behavior. *Nat*
328 *Neurosci* **22**, 2040-2049 (2019).
329 12. Dickinson, M.H. & Tu, M.S. The function of dipteran flight muscle. *Comparative Biochemistry and Physiology Part A:*
330 *Physiology* **116**, 223-238 (1997).
331 13. Ewing, A.W. The neuromuscular basis of courtship song in Drosophila: The role of the direct and axillary wing muscles.
332 *Journal of comparative physiology* **130**, 87-93 (1979).
333 14. O'Sullivan, A.*, et al.* Multifunctional Wing Motor Control of Song and Flight. *Curr Biol* **28**, 2705-2717.e2704 (2018).
334 15. Phelps, J.S.*, et al.* Reconstruction of motor control circuits in adult Drosophila using automated transmission electron
335 microscopy. *Cell* **184**, 759-774.e718 (2021).
336 16. Shirangi, T.R., Stern, D.L. & Truman, J.W. Motor control of Drosophila courtship song. *Cell Rep* **5**, 678-686 (2013).
337 17. Bath, D.E.*, et al.* FlyMAD: rapid thermogenetic control of neuronal activity in freely walking Drosophila. *Nat Methods* **11**,
338 756-762 (2014).
339 18. Coen, P., Xie, M., Clemens, J. & Murthy, M. Sensorimotor Transformations Underlying Variability in Song Intensity during
340 Drosophila Courtship. *Neuron* **89**, 629-644 (2016).
341 19. Inagaki, H.K.*, et al.* Optogenetic control of Drosophila using a red-shifted channelrhodopsin reveals experience-dependent
342 influences on courtship. *Nat Methods* **11**, 325-332 (2014).
343 20. Roemschied, F.A.*, et al.* Flexible Circuit Mechanisms for Context-Dependent Song Sequencing. *bioRxiv*,
344 2021.2011.2001.466727 (2021).
345 21. von Philipsborn, A.C.*, et al.* Neuronal control of Drosophila courtship song. *Neuron* **69**, 509-522 (2011).

346 22. Clyne, J.D. & Miesenböck, G. Sex-specific control and tuning of the pattern generator for courtship song in Drosophila.
347 *Cell* **133**, 354-363 (2008).
348 23. Shirangi, T.R., Wong, A.M., Truman, J.W. & Stern, D.L. Doublesex Regulates the Connectivity of a Neural Circuit
349 Controlling Drosophila Male Courtship Song. *Dev Cell* **37**, 533-544 (2016).
350 24. Yu, J.Y., Kanai, M.I., Demir, E., Jefferis, G.S. & Dickson, B.J. Cellular organization of the neural circuit that drives
351 Drosophila courtship behavior. *Curr Biol* **20**, 1602-1614 (2010).
352 25. Luan, H., Peabody, N.C., Vinson, C.R. & White, B.H. Refined spatial manipulation of neuronal function by combinatorial
353 restriction of transgene expression. *Neuron* **52**, 425-436 (2006).
354 26. Pfeiffer, B.D.*, et al.* Refinement of tools for targeted gene expression in Drosophila. *Genetics* **186**, 735-755 (2010).
355 27. Klapoetke, N.C.*, et al.* Independent optical excitation of distinct neural populations. *Nat Methods* **11**, 338-346 (2014).
356 28. Ewing, A.W. The neuromuscular basis of courtship song inDrosophila: The role of the indirect flight muscles. *Journal of*
357 *comparative physiology* **119**, 249-265 (1977).
358 29. Clowney, E.J., Iguchi, S., Bussell, J.J., Scheer, E. & Ruta, V. Multimodal Chemosensory Circuits Controlling Male
359 Courtship in Drosophila. *Neuron* **87**, 1036-1049 (2015).
360 30. Kallman, B.R., Kim, H. & Scott, K. Excitation and inhibition onto central courtship neurons biases Drosophila mate choice.
361 *Elife* **4**, e11188 (2015).
362 31. Kohatsu, S., Koganezawa, M. & Yamamoto, D. Female contact activates male-specific interneurons that trigger stereotypic
363 courtship behavior in Drosophila. *Neuron* **69**, 498-508 (2011).
364 32. Kohatsu, S. & Yamamoto, D. Visually induced initiation of Drosophila innate courtship-like following pursuit is mediated
365 by central excitatory state. *Nat Commun* **6**, 6457 (2015).
366 33. Zhou, C.*, et al.* Central neural circuitry mediating courtship song perception in male Drosophila. *Elife* **4** (2015).
367 34. Dana, H.*, et al.* High-performance calcium sensors for imaging activity in neuronal populations and microcompartments.
368 *Nat Methods* **16**, 649-657 (2019).
369 35. Hige, T., Aso, Y., Rubin, G.M. & Turner, G.C. Plasticity-driven individualization of olfactory coding in mushroom body
370 output neurons. *Nature* **526**, 258-262 (2015).
371 36. Rideout, E.J., Dornan, A.J., Neville, M.C., Eadie, S. & Goodwin, S.F. Control of sexual differentiation and behavior by the
372 doublesex gene in Drosophila melanogaster. *Nat Neurosci* **13**, 458-466 (2010).
373 37. Court, R.*, et al.* A Systematic Nomenclature for the Drosophila Ventral Nerve Cord. *Neuron* **107**, 1071-1079.e1072 (2020).
374 38. Namiki, S., Dickinson, M.H., Wong, A.M., Korff, W. & Card, G.M. The functional organization of descending sensory-
375 motor pathways in Drosophila. *Elife* **7** (2018).
376 39. Auer, T.O. & Benton, R. Sexual circuitry in Drosophila. *Curr Opin Neurobiol* **38**, 18-26 (2016).
377 40. Stockinger, P., Kvitsiani, D., Rotkopf, S., Tirián, L. & Dickson, B.J. Neural circuitry that governs Drosophila male courtship
378 behavior. *Cell* **121**, 795-807 (2005).
379 41. Lacin, H.*, et al.* Neurotransmitter identity is acquired in a lineage-restricted manner in the Drosophila CNS. *Elife* **8** (2019).
380 42. EWING, A.W. The role of feedback during singing and flight in Drosophila melanogaster. *Physiological entomology* **4**,
381 329-337 (1979).

43. Peña, F., Parkis, M.A., Tryba, A.K. & Ramirez, J.-M. Differential contribution of pacemaker properties to the generation of respiratory rhythms during normoxia and hypoxia. *Neuron* **43**, 105-117 (2004).

44. St John, W., Zhou, D. & Fregosi, R.F. Expiratory neural activities in gasping. *Journal of Applied Physiology* **66**, 223-231 (1989).

45. Feng, K.*, et al.* Distributed control of motor circuits for backward walking in Drosophila. *Nature communications* **11**, 1-17 (2020).

46. Tirian, L. & Dickson, B.J. The VT GAL4, LexA, and split-GAL4 driver line collections for targeted expression in the Drosophila nervous system. *bioRxiv*, 198648 (2017).

47. Nern, A., Pfeiffer, B.D. & Rubin, G.M. Optimized tools for multicolor stochastic labeling reveal diverse stereotyped cell arrangements in the fly visual system. *Proceedings of the National Academy of Sciences* **112**, E2967-E2976 (2015).

48. Belote, J.M. & Baker, B.S. Sex determination in Drosophila melanogaster: analysis of transformer-2, a sex-transforming locus. *Proceedings of the National Academy of Sciences* **79**, 1568-1572 (1982).

49. Pfeiffer, B.D.*, et al.* Tools for neuroanatomy and neurogenetics in Drosophila. *Proceedings of the National Academy of Sciences* **105**, 9715-9720 (2008).

50. Bohm, R.A.*, et al.* A genetic mosaic approach for neural circuit mapping in Drosophila. *Proceedings of the National Academy of Sciences* **107**, 16378-16383 (2010).

51. Otsuna, H., Ito, M. & Kawase, T. Color depth MIP mask search: a new tool to expedite Split-GAL4 creation. *bioRxiv*, 318006 (2018).

52. Talay, M.*, et al.* Transsynaptic Mapping of Second-Order Taste Neurons in Flies by trans-Tango. *Neuron* **96**, 783-795.e784 (2017).

53. Arthur, B.J., Sunayama-Morita, T., Coen, P., Murthy, M. & Stern, D.L. Multi-channel acoustic recording and automated analysis of Drosophila courtship songs. *BMC Biol* **11**, 11 (2013).

54.Shiozaki, H.M. & Kazama, H. Parallel encoding of recent visual experience and self-motion during navigation in Drosophila. *Nat Neurosci* **20**, 1395-1403 (2017).

55. Aso, Y.*, et al.* The neuronal architecture of the mushroom body provides a logic for associative learning. *Elife* **3**, e04577 (2014).

56. Arthur, B.J.*, et al.* SongExplorer: A deep learning workflow for discovery and segmentation of animal acoustic communication signals. *bioRxiv*, 2021.2003.2026.437280 (2021).

57. Pnevmatikakis, E.A. & Giovannucci, A. NoRMCorre: An online algorithm for piecewise rigid motion correction of calcium imaging data. *J Neurosci Methods* **291**, 83-94 (2017).

58. Rohlfing, T. & Maurer, C.R., Jr. Nonrigid image registration in shared-memory multiprocessor environments with application to brains, breasts, and bees. *IEEE Trans Inf Technol Biomed* **7**, 16-25 (2003).

Methods

Fly husbandry. Flies (*Drosophila melanogaster*) were raised on cornmeal-molasses food at 23 °C under a 12-h/12-h light-dark cycle until eclosion. In all experiments, we used 5–7 days old adult male flies collected within 6 hours after eclosion and maintained in isolation in the dark. For the adult male flies used in experiments involving optogenetic stimulation, the food was supplemented with 0.4 mM all-trans-retinal (Toronto Research Chemicals). Virgin female flies used in behavioral experiments were housed in groups of approximately twenty.

Fly stocks and genotypes. Fly stocks used in this study are as follows: w^{1118} (Stern Laboratory); UAS-CsChrimson-tdTomato(VK00005)[27] (a gift from Gerald Rubin); VT037566-p65ADZp(attP40)[45, 46] (Dickson Laboratory); VT041688-ZpGDBD(attP2)[46] (Bloomington Drosophila Stock Center; BDSC #72408); VT042732-p65ADZp(attP40)[46] (BDSC #71534); dsx-ZpGDBD[23]; UAS-CsChrimson-mVenus(attP18)[27] (BDSC #55134); w^{1118},hsFLPG5.PEST(attP3);;UAS-FRT.stop-myr::smGdP-HA(VK00005),UAS-FRT.stop-myr::smGdP-V5-THS-UAS-FRT.stop-myr::smGdP-FLAG(su(Hw)attP1)[47] (BDSC #64085); R22D03-LexA(attP2)[26] (a gift from Gerald Rubin); LexAop2-CsChrimson-tdTomato(VK00005)[27] (a gift from Vivek Jayaraman); UAS-IVS-jGCaMP7f(su(Hw)attP5)[34] (BDSC #80906); UAS-IVS-myr::tdTomato(attP40)[26] (BDSC #32222); VT040556-p65ADZp(attP40)[3, 46] (BDSC #72060); VT040347-ZpGDBD(attP2)[3, 46] (BDSC #75302); VT040347-ZpLexADBD(attP2)[46] (Dickson Laboratory); UAS-IVS-jGCaMP7s(su(Hw)attP5)[34] (BDSC #80905); dsx-Gal4[48] (a gift from Bruce Baker); R57C10-LexA(attP40)[26] (BDSC #52817); UAS-CsChrimson-tdTomato(su(Hw)attP5)[27] (a gift from Vivek Jayaraman); LexAop2-IVS-jGCaMP7s(VK00005)[34] (BDSC #80913); R57C10-Gal4(attP2)[49] (BDSC #39171); fru-Gal4[40] (BDSC #66696); fru-Flp[24]; tubP-FRT.stop-Gal80;MKRS/TM6B[50] (BDSC #38878); R57C10-Gal4(attP40)[49] (a gift from Gerald Rubin).

The dPR1 and TN1A split-Gal4 drivers were generated from the following split lines: dPR1 from SS65789 (VT037566-p65ADZp(attP40); VT041688-ZpGDBD(attP2)); TN1Afrom SS59832 (VT042732-p65ADZp(attP40);dsx-ZpGDBD/TM6b). These lines were identified by screening split lines identified by color depth MIP search[51] of candidate *fru*-expressing neurons and neurons identified with trans-Tango[52] applied to a pIP10 split-Gal4 line[3].

The genotypes of the flies used in each figure are as follows. Fig. 1a, w^{1118}/Y;;UAS-CsChrimson-tdTomato(VK00005)/+; Fig. 1b, Extended Data Fig. 1a,c,d, and Extended Data Fig. 7c,d, w^{1118},UAS-CsChrimson-mVenus(attP18)/Y;VT037566-p65ADZp(attP40)/+;VT041688-ZpGDBD(attP2)/+, w;VT042732-p65ADZp(attP40)/+;dsx-ZpGDBD/UAS-CsChrimson-tdTomato(VK00005); Fig. 1d–i, Extended Data Fig. 1g–l, and Extended Data Fig. 2d–f, VT037566-p65ADZp(attP40)/+;VT041688-ZpGDBD(attP2)/UAS-CsChrimson-tdTomato(VK00005), VT042732-p65ADZp(attP40)/+;dsx-ZpGDBD/UAS-CsChrimson-tdTomato(VK00005); Extended Data Fig. 1b, w^{1118},hsFLPG5.PEST(attP3)/Y;VT037566-p65ADZp(attP40)/+;UAS-FRT.stop-myr::smGdP-HA(VK00005),UAS-FRT.stop-myr::smGdP-V5-THS-UAS-FRT.stop-myr::smGdP-FLAG(su(Hw)attP1)/VT041688-ZpGDBD(attP2); Extended Data Fig. 1e, w^{1118},hsFLPG5.PEST(attP3)/Y; VT042732-p65ADZp(attP40)/+;UAS-FRT.stop-myr::smGdP-HA(VK00005),UAS-FRT.stop-myr::smGdP-V5-THS-UAS-FRT.stop-myr::smGdP-FLAG(su(Hw)attP1)/dsx-ZpGDBD; Extended Data Fig. 1m–o and Extended Data Fig. 2a–c, w^{1118}/Y;;UAS-CsChrimson-tdTomato(VK00005)/+, w^{1118}/Y;VT037566-p65ADZp(attP40)/+;VT041688-ZpGDBD(attP2)/+,

452 w^{1118}/Y;VT042732-p65ADZp(attP40)/+;dsx-ZpGDBD/+; Fig. 2b and Extended Data Fig. 3a, R22D03-
453 LexA(attP2)/LexAop2-CsChrimson-tdTomato(VK00005); Fig. 2c and Extended Data Fig. 3b–e, UAS-IVS-
454 jGCaMP7f(su(Hw)attP5),UAS-IVS-myr::tdTomato(attP40)/+;R22D03-LexA(attP2),LexAop2-CsChrimson-
455 tdTomato(VK00005)/+; Fig. 2d–h, Extended Data Fig. 4a–g,o, and Extended Data Fig. 6a,b, UAS-IVS-
456 jGCaMP7f(su(Hw)attP5),UAS-IVS-myr::tdTomato(attP40)/VT037566-p65ADZp(attP40);R22D03-
457 LexA(attP2),LexAop2-CsChrimson-tdTomato(VK00005)/VT041688-ZpGDBD(attP2); Fig. 2i–l, \Extended Data Fig.
458 4h–n,p, and Extended Data Fig. 6b, UAS-IVS-jGCaMP7f(su(Hw)attP5),UAS-IVS-myr::tdTomato(attP40)/VT042732-
459 p65ADZp(attP40);R22D03-LexA(attP2),LexAop2-CsChrimson-tdTomato(VK00005)/dsx-ZpGDBD; Extended Data
460 Fig. 3d, w^{1118}/Y;;UAS-CsChrimson-tdTomato(VK00005)/+; Extended Data Fig. 3f,g, VT040556-
461 p65ADZp(attP40)/+;VT040347-ZpGDBD(attP2)/UAS-CsChrimson-tdTomato(VK00005); Extended Data Fig. 5a,b,
462 VT040556-p65ADZp(attP40),UAS-IVS-jGCaMP7s(su(Hw)attP5)/VT040556-p65ADZp(attP40);VT040347-
463 ZpLexADBD(attP2),LexAop2-CsChrimson-tdTomato(VK00005)/VT040347-ZpGDBD(attP2); Extended Data Fig.
464 5c,f, VT040556-p65ADZp(attP40)/+;VT040347-ZpLexADBD(attP2)/LexAop2-CsChrimson-tdTomato(VK00005);
465 Extended Data Fig. 5e, w^{1118}/Y;;LexAop2-CsChrimson-tdTomato(VK00005)/+; Extended Data Fig. 5f,
466 w^{1118}/Y;VT040556-p65ADZp(attP40)/+;VT040347-ZpLexADBD(attP2)/+; Extended Data Fig. 5g,h,k–m and
467 Extended Data Fig. 6e–j, VT040556-p65ADZp(attP40),UAS-IVS-jGCaMP7s(su(Hw)attP5)/+;VT040347-
468 ZpLexADBD(attP2),LexAop2-CsChrimson-tdTomato(VK00005)/dsx-Gal4; Extended Data Fig. 5i,j,n–p, VT040556-
469 p65ADZp(attP40),UAS-IVS-jGCaMP7s(su(Hw)attP5)/VT042732-p65ADZp(attP40);VT040347-
470 ZpLexADBD(attP2),LexAop2-CsChrimson-tdTomato(VK00005)/dsx-ZpGDBD; Fig. 3 and Extended Data Fig. 6c,d,
471 UAS-IVS-jGCaMP7f(su(Hw)attP5),UAS-IVS-myr::tdTomato(attP40)/+;R22D03-LexA(attP2),LexAop2-CsChrimson-
472 tdTomato(VK00005)/dsx-Gal4; Fig. 4c and Extended Data Fig. 7a,b, VT037566-p65ADZp(attP40),UAS-CsChrimson-
473 tdTomato(su(Hw)attP5)/R57C10-LexA(attP40);VT041688-ZpGDBD(attP2),LexAop2-IVS-jGCaMP7s(VK00005)/+,
474 VT042732-p65ADZp(attP40),UAS-CsChrimson-tdTomato(su(Hw)attP5)/R57C10-LexA(attP40);dsx-
475 ZpGDBD/LexAop2-IVS-jGCaMP7s(VK00005); Fig. 4e–h, Extended Data Fig. 8, and Extended Data Fig. 9g,h, UAS-
476 IVS-jGCaMP7f(su(Hw)attP5),UAS-IVS-myr::tdTomato(attP40)/+;R22D03-LexA(attP2),LexAop2-CsChrimson-
477 tdTomato(VK00005)/R57C10-Gal4(attP2); Fig. 5b–e and Extended Data Fig. 9a–f, UAS-IVS-
478 jGCaMP7f(su(Hw)attP5),UAS-IVS-myr::tdTomato(attP40)/+;R22D03-LexA(attP2),LexAop2-CsChrimson-
479 tdTomato(VK00005)/fru-Gal4; Fig. 5g–i and Extended Data Fig. 9g,h, UAS-IVS-jGCaMP7f(su(Hw)attP5)/R57C10-
480 Gal4(attP40),tubP-FRT.stop-Gal80;R22D03-LexA(attP2),LexAop2-CsChrimson-tdTomato(VK00005)/fru-Flp.
481

482 **Behavioral experiments.** Song recordings in freely moving flies were conducted using the multi-channel song
483 recording system described previously[53]. Briefly, the system is composed of 5-mm behavioral chambers, each equipped
484 with a microphone (CMP5247TF-K, CUI Devices). The output of the microphones was recorded at 5 kHz. Temperature
485 and relative humidity were maintained at 23°C and 50%, respectively. For optogenetic stimulation, an array of red
486 LEDs (630-nm) (NFLS-R300X3-WHT-LC2, Super Bright LEDs) was placed approximately 15 mm from the tops of
487 the chambers. During the recordings, the chambers were constantly illuminated with an ambient blue light (1.4

488 μW/mm^2) (STN-BBLU-A3A-10B5M-12V, Super Bright LEDs) to enable flies to perform visually guided behaviors
489 such as orientation toward females.
490 Flies were transferred from culture vials to the chambers with an aspirator without anesthesia. For the single fly
491 optogenetic activation experiment, one male fly was placed in each chamber. For each trial, continuous light
492 stimulation at a fixed power was applied for 10 s with an inter-trial interval of 20 s. Light power varied from trial-to-
493 trial (6 levels between 4.0 and 39.7 μW/mm^2) in a randomized order. Stimulation of each light power was repeated in 6
494 trials. For the paired fly optogenetic activation experiment, one male and one virgin female flies were placed in each
495 chamber. For each trial, constant light stimulation, whose power varied from trial-to-trial (4.0, 7.9, or 11.9 μW/mm^2),
496 was applied for 5 s with an inter-trial interval of 10 s. Stimulation of the same light power was applied in 24 trials.
497
498 **Calcium imaging.** Flies were prepared for calcium imaging using the protocol described previously[54] with
499 modifications. Briefly, flies were placed on a Peltier plate that maintained temperature at 4 °C. The proboscis was fixed
500 to the head capsule with UV glue, and the middle and hind legs were cut around the femur-trochanter junctions. The
501 flies were then attached to a custom holding plate upside down (Fig. 2a) by applying the glue to the coxa and trochanter
502 of the middle legs and femur of the forelegs. The thorax was largely free from the glue so as not to disturb thorax
503 oscillations and thus wing movement. The cuticles and apodemes covering the pro- and meso-thoracic ganglia were
504 removed with fine forceps. The dissection was performed in saline (103 mM NaCl, 3 mM KCl, 5 mM N-
505 tris(hydroxymethyl) methyl-2aminoethane-sulfonic acid, 8 mM trehalose, 10 mM glucose, 26 mM $NaHCO_3$, 1 mM
506 NaH_2PO_4, 1.5 mM $CaCl_2$, and 4 mM $MgCl_2$; pH, 7.1–7.3; osmolarity, 270-275 mOsm) bubbled with carbogen (95% O_2
507 and 5% CO_2).
508 Calcium imaging was conducted using a two-photon microscope (Bergamo II, Thorlabs) with a pulsed laser tuned
509 to 940 nm (InSight X3, Spectra-Physics). The laser power measured under the objective lens was kept below 25 mW. A
510 piezo actuator (PFM450E, Thorlabs) was used to move an objective lens (N16XLWD-PF, Nikon) for data acquisition
511 from multiple z-planes. For experiments with optogenetic activation of pIP10, dPR1, or TN1A, two-dimensional
512 images (512 × 512 pixels, pixel size 0.49 um) were taken from 30 z-planes (4 um step) at 1.4 volumes per s. For
513 experiments with optogenetic activation of the song driver, images (256 × 256 pixels, pixel size 0.25–0.79 um) were
514 taken from 10 z-planes (4 um step) at 7.1 volumes per s. In the recording from single dPR1 neurons, imaged volumes
515 contained cell body signals in both hemispheres in most of the experiments. In the recording from single TN1A and
516 TN1 neurons, imaged volumes contained cell body signals of most of the target neurons in one hemisphere. In a subset
517 of recordings where neurons expressed tdTomato in addition to GCaMP, signals of both fluorescent proteins were
518 recorded simultaneously. Carbogenated saline was perfused throughout the recording.
519 During calcium imaging, optogenetic activation light (660-nm) (S1FC660, Thorlabs) passed through a long-pass
520 filter (FEL0650, Thorlabs) and was delivered with a patch cable (M125L01, Thorlabs) placed at 6 mm away from the
521 fly. For each fly, a continuous light stimulation at a fixed power was applied for 10 s with an inter-trial interval of 20 s.
522 The light power varied from trial-to-trial (6 levels, 4.9–156.2 μW/mm^2 for pIP10, dPR1, and TN1A stimulations, 4.9–
523 17.1 μW/mm^2 for song driver stimulation) in a randomized order. Stimulation of the same power was repeated in 6

trials for song driver stimulation and 3 trials for pIP10 stimulation. For the pIP10 and song driver simulations in tethered flies without calcium imaging, the light power ranged from 2.4 to 14.6 μW/mm^2. The same stimulus was presented in 6 trials.

The sound of vibrating wings was recorded with a pair of microphones (NR-23158, Knowles) placed near the left and right wings, respectively. Microphone signals were amplified with a custom amplifier[53] and recorded at 10 kHz. Wing movement was monitored with a camera (BFS-U3-04S2M-CS, Teledyne FLIR) equipped with a periscopic lens (InfiniStix 90°, working distance 94 mm, magnification 1.0×, Infinity). Flies were illuminated by infrared light (850-nm) (M850F2, Thorlabs) with a patch cable (M125L01, Thorlabs). A long-pass (FEL0800, Thorlabs) and a short-pass (FES0850, Thorlabs) filter were placed on the lens to remove the optogenetic and two-photon activation light, respectively. Video was recorded at 100 frames per s.

Immunohistochemistry. The dissections, immunohistochemistry, and imaging of fly central nervous systems were performed using protocols described previously[47, 55] (https://www.janelia.org/project-team/flylight/protocols) with modifications. Briefly, brains and VNCs were dissected in Schneider's insect medium and fixed in 2% paraformaldehyde at room temperature for 55 min. Tissues were washed in PBT (0.5% Triton X-100 in phosphate buffered saline) and blocked using 5% normal goat serum before incubation with antibodies.

To visualize the expression pattern of GFP or GCaMP, tissues were stained using rabbit anti-GFP (1:1000, A-11122, Thermo Fisher Scientific) and mouse nc82 (1:30, Developmental Studies Hybridoma Bank) as primary antibodies and Alexa Fluor 488-conjugated goat anti-rabbit (A-11034, Thermo Fisher Scientific) and Alexa Fluor 568-conjugated goat anti-mouse (A-11031, Thermo Fisher Scientific) as secondary antibodies. To visualize the expression pattern of tdTomato, tissues were stained using rabbit anti-dsRed (1:1000, #632496, Clontech) and mouse nc82 (1:30) as primary antibodies and Cy3-conjugated goat anti-rabbit (#111-165-144, Jackson ImmunoResearch) and Cy2-conjugated goat anti-mouse (#115-225-166, Jackson ImmunoResearch) as secondary antibodies. To visualize the expression pattern of GCaMP and tdTomato in the same samples, tissues were stained using chicken anti-GFP (1:1000, A-10262, Thermo Fisher Scientific), rabbit anti-dsRed (1:1000), and mouse nc82 (1:30) as primary antibodies and Alexa Fluor 488-conjugated goat anti-chicken (A32931, Thermo Fisher Scientific), Cy3-conjugated goat anti-rabbit, and Cy5-conjugated goat anti-mouse (#115-175-166, Jackson ImmunoResearch) as secondary antibodies. To visualize the expression pattern of *dsx*, tissues were stained using mouse anti-DsxDBD (1:2, Developmental Studies Hybridoma Bank), rabbit anti-GFP (1:1000), and rat anti-DN-Cadherin (1:100, DN-Ex #8, Developmental Studies Hybridoma Bank) as primary antibodies and Cy3-conjugated goat anti-mouse (#115-165-166, Jackson ImmunoResearch), Alexa Fluor 488-conjugated goat anti-rabbit, and Cy5-conjugated goat anti-rat (#112-175-167, Jackson ImmunoResearch) as secondary antibodies. Flies for multi-color flip out[47] underwent a 40-min heat shock during 0–1 day post eclosion and dissected at 5–14 days old. These tissues were stained with the antibodies described previously[47].

Image stacks were collected using a confocal microscope (LSM710, Zeiss, Germany) with an objective lens (Plan-Apochromat 20x/0.8 M27 or Plan-Apochromat 40X/1.3 M27, Zeiss, Germany).

Song type classification. Pulse and sine songs were detected using SongExplorer[56], a deep-learning based algorithm for segmenting acoustic communication signals. We first removed low-frequency components of the microphone signals (<100 Hz), which were mostly irrelevant for song, using continuous wavelet transformation. We then performed manual annotation for a subset of the audio data. For the data obtained from freely moving flies, we used the labels "pulse", "sine", "inter-pulse intervals", "others" for non-song sounds (e.g., noise during grooming), and "ambient." Another label "flight" was added for the data from tethered flies because these flies occasionally showed flight-like wing movement. We then trained a classifier separately for freely moving and tethered flies using the annotated data. These classifiers were applied to assign a label at every 1.6 ms of the data from all the recordings. The classification accuracies, measured with cross-validation, for the data from freely moving and tethered flies were 91.6% and 88.1%, respectively. Visual inspection of the classifier predictions revealed that misclassifications often occurred at a smaller number of consecutive time bins compared with correct predictions. To correct for these misclassifications, we smoothed the time series of classifier predictions with median filters (the window size for detecting "pulse", 17.6 ms; "sine", 25.6 ms; "flight", 80 ms).

To compare the amounts of pulse and sine song, we calculated the pulse train based on the classifier predictions. Pulse song is composed of discrete pulse events separated by inter-pulse intervals, whereas sine song is continuous. We defined the pulse train by merging pulse events with inter-pulse intervals of 50 ms or shorter. This allows comparisons of the amounts of pulse and sine song on the same scale. Events designated as "pulse" in the figures represent the pulse train.

Data analysis for behavioral experiments. For each recording, we calculated the time series of the proportions of pulse and sine song by combining data across repeated presentations of the same optogenetic stimulus. These time series were averaged across flies to obtain the time course of song proportions, or across time to calculate the song probabilities for each fly. For the paired fly optogenetic activation experiment, we quantified how much optogenetic stimulation changed the amounts of pulse and sine song by subtracting the proportions of pulse and sine song during optogenetic stimulation from those during 5-s pre-stimulation periods. We also quantified the probabilities of song initiation, song termination, and song type switch based on the song type classifier's output (Extended Data Fig. 2d–f). For each fly, we aggregated data from the same optogenetic stimulation level and calculated these probabilities at each time bin. For the analysis of song initiation, we detected the "ambient" events and calculated the probabilities of observing "pulse" and "sine" events in the following time bin. The probabilities of pulse song termination were calculated by detecting the "pulse" events and calculated the probabilities of observing "ambient" events in the following time bin. The probabilities of pulse to sine transitions were computed using the same method except that "ambient" events were replaced with "sine" events. The probability of sine song termination and sine to pulse transitions were calculated similarly.

Data analysis for calcium imaging experiments. Time series of z-stack images underwent rigid motion correction with the NoRMCorre algorithm[57]. To analyze calcium signals of dPR1 cell bodies, we first set a volume of interest

596 (VOI) separately for the dPR1 neuron in each hemisphere. We then calculated an average intensity z-projection of the
597 VOI and performed another round of rigid motion correction. The same procedure was carried out for analyzing TN1A
598 cell bodies, dPR1 neurite, and TN1A neurite, except that a single volume of interest was used to calculate an average
599 intensity z-projection. For each recording, regions of interest (ROIs), each corresponding to a cell body or target
600 neurites, were manually defined using an average image of the motion corrected z-projections. Signals in each ROI
601 were averaged for further analysis. Motion corrections were performed using either GCaMP or tdTomato signals. For
602 analyzing data from pan-neuronal and *fru*-expressing neuron imaging, the motion corrected z-stack images went
603 through 2 by 2 voxel binning in the xy-planes to increase the signal-to-noise ratio. ΔF/F was calculated for each ROI or
604 voxel by defining the baseline as the mean fluorescent signal during 10-s periods preceding optogenetic stimulation.
605 To compare spatial activity patterns across flies, inter-fly image registration was performed for the data from pan-
606 neuronal and *fru*-expressing neuron imaging. First, the motion corrected z-stack images were averaged across time for
607 each recording. Second, the averaged z-stack images went through 2 by 2 voxel binning in the xy-planes. Third, the
608 binned images from one recording were selected as a reference for each target volume (e.g., a dorsal volume) and each
609 driver line (e.g., the pan-neuronal line). Finally, the time-averaged z-stack images of each recording were aligned to the
610 reference with either the NoRMCorre rigid registration or the Computational Morphometry Toolkit[58] run with a Fiji
611 plugin (https://github.com/jefferis/fiji-cmtk-gui). These registration parameters were used to calculate population
612 averaged calcium response patterns.
613 To analyze the relationship between calcium signals and song, we converted the sampling rate of song classifier
614 predictions (625 Hz) to that of calcium imaging (7.1 Hz; sampling at every 141 ms) as follows. Time series of the
615 predictions were separated into 141-ms bins, and the mean probabilities of each event ("pulse", "sine", "ambient", and
616 "flight) were calculated for each bin. We considered that an event occurred in a bin if the probability exceeded a
617 threshold (0.1 for "pulse", 0.6 for "sine, 0.9 for "ambient", 0.01 for "flight"). Defining event occurrence with these
618 thresholds rarely gave false positives when assessed with visual inspection. Flight-like behavior induced changes in
619 calcium signals in a large fraction of the imaged volume (data not shown), which can obscure song-related calcium
620 signals. We therefore excluded from further analysis the data during "flight" and from -1 to 1 s after "flight".
621 To characterize the changes in calcium signals during song-type transitions, we first calculated the average ΔF/F in
622 the two bins over which song type was changed (from 141 ms before the transition to 141 ms after the transition). We
623 then subtracted this value from the average ΔF/F in the third and fourth bins after the change in song type (282–423 ms
624 after the transition). Considering the kinetics of jGCaMP7f[34], this quantity likely reflects changes in neural activity
625 during song type transitions. To characterize the changes in calcium signals during quiet to pulse transitions, we
626 detected "pulse" bins that followed at least 2-s continuous "ambient" periods. The changes in ΔF/F during the
627 transitions were defined as the subtraction of the average ΔF/F during the 2-s period before the transition from that after
628 the transition. We analyzed the data from the recordings where the transitions occurred at least five times for the
629 analysis of song type transitions and two times for the analysis of quiet to pulse transitions. We focused on song type
630 transitions rather than calcium signals during each song type because pulse and sine song tended to occur in different
631 timings in 10-s stimulation periods, and thus factors irrelevant for song (e.g., time-varying input from song irrelevant

632 CsChrimson expressing neurons) can contribute to the differential calcium signals during pulse and sine song.
633 To assess whether individual TN1 neurons responded to optogenetic stimulation, we calculated the mean ΔF/F
634 during the stimulation period subtracted from that of the 10-s pre-stimulation period for each trial for a range of
635 stimulation levels (9.8–17.1 μW/mm^2 for song driver stimulation; 19.5–156.2 μW/mm^2 for pIP10 stimulation). We then
636 aggregated the responses across stimulation levels and performed one-sample t-test.
637 For single dPR1, TN1A, and TN1 neurons, the preference for song type was quantified using the receiver operating
638 characteristics (ROC) analysis (Extended Data Fig. 6a). We first built the distribution of the changes in ΔF/F separately
639 for pulse-to-sine and sine-to-pulse transitions. We then used the two distributions to calculate the area under the ROC
640 curve. An index termed the song-type preference was defined as the AUC scaled from −1 to 1. This index quantifies
641 how much the type of transitions (pulse-to-sine vs. sine-to-pulse) can be predicted based on the changes in calcium
642 signals. A song-type preference of 1 and -1 represents perfect predictions with higher calcium signals for pulse and sine
643 song, respectively. A song-type preference of 0 indicates that the changes in calcium signals were indistinguishable
644 between the two types of transitions. For single TN1A neurons, we assessed whether the song-type preference was
645 different from 0 using a permutation test. We shuffled the labels (i.e., pulse-to-sine and sine-to-pulse transitions) of
646 transition responses and calculated song-type preference. This was repeated 10,000 times to obtain a null distribution of
647 song-type preference. The same permutation test was conducted for each voxel for the data obtained in pan-neuronal
648 and *fru*-expressing neuron imaging (Extended Data Figs. 8 and 9). For these data, we also calculated a null distribution
649 of transition responses for each voxel using permutation (Extended Data Figs. 8 and 9). We first randomized the
650 relationship between song type transitions and calcium signals by shuffling the trials for calcium signal data. We then
651 calculated the distribution of transition responses as in the original data.
652 Images involved in calcium signals were spatially smoothed with a 2-D Gaussian filter for presentation in figures.
653
654 **Statistics.** All statistical tests were two-tailed and performed using MATLAB 2022b.

Data availability

Data are available at FigShare.

Code availability

Code is available at FigShare.

Acknowledgments

We thank A. Leonard, V. Goncharov, and J. Arnold for help setting up the two-photon microscope, S. Sawtelle, B. Arthur, and E. Behrman for help with song recording, B. Arthur for help with SongExplorer, the Janelia Project Technical Resources team (C. Christoforou, K. Klose, Y. He, and J. Hausenfluck, led by G. Ihrke) and the FlyLight team for performing dissections, histological preparations, and confocal imaging in immunohistochemical experiments, Z. Dorman, G. W. Meissner, and G. Ihrke for help with multi-color flip out experiment designs, H. Otsuna for help with split-Gal4 line generation, G. M. Rubin and V. Jayaraman for fly stocks, V. Ruta for comments on the manuscript, and members of the Stern lab for valuable discussions. This article is subject to HHMI's Open Access to Publications policy. HHMI lab heads have previously granted a nonexclusive CC BY 4.0 license to the public and a sublicensable license to HHMI in their research articles. Pursuant to those licenses, the author-accepted manuscript of this article can be made freely available under a CC BY 4.0 license immediately upon publication.

Author contributions

H.M.S. and D.L.S. conceived the study. H.M.S. performed all experiments and analyzed data. H.M.S., K.W., J.L.L., M.S., and B.J.D. generated genetic reagents. H.M.S. and D.L.S. wrote the manuscript with input from K.W., J.L.L., and B.J.D.

Competing interests

The authors declare no competing interests.

Supplementary information

Supplementary Video 1

An example trial of calcium imaging in dPR1 neurons. Top left: a bottom view of the fly. The left side of the image corresponds to the right side of the fly. Bottom left: the microphone signal for the right wing. Top right: raw fluorescent signals (F) averaged across z-planes. The left side of the image corresponds to the left side of the VNC. Top left: schematic of the imaged volume. Red boxes represent the timing of optogenetic stimulation.

Supplementary Video 2

An example trial of calcium imaging in TN1A neurons. Same format as in Supplementary Video 1.

Supplementary Video 3

An example trial of pan-neuronal calcium imaging in dPR1 neurons. Top left: the microphone signal for the right wing. The red box represents the timing of optogenetic stimulation. Bottom left: schematic of the imaged volume. Right: raw fluorescent signals (F) for each z-plane.

Supplementary Video 4

Same as in Supplementary Video 3 but for calcium signals averaged across z-planes.

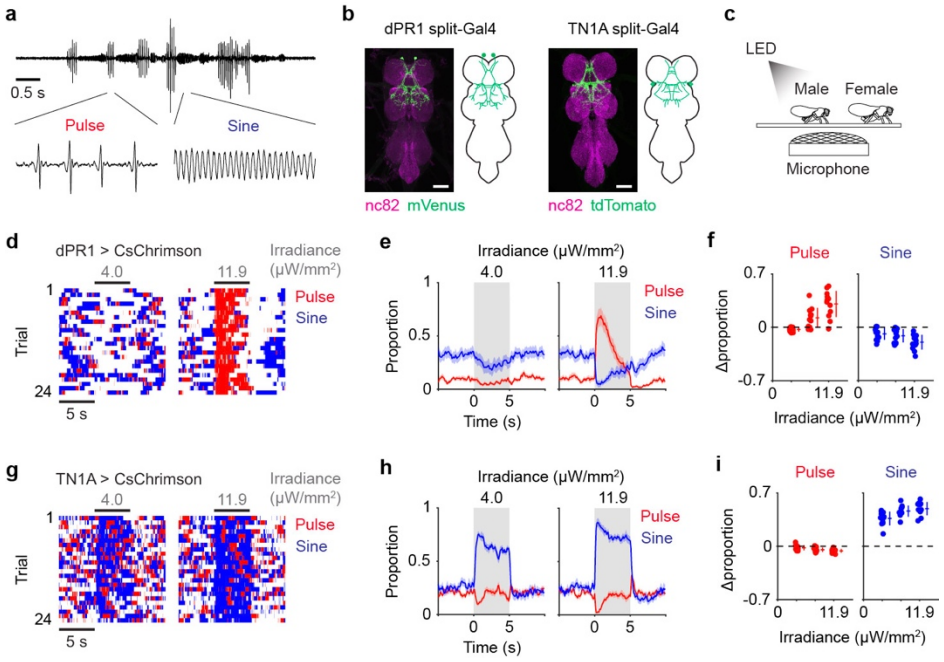

Fig. 1 | Optogenetic activation of dPR1 and TN1A modulates pulse and sine song production in distinct ways. a, A recording of the sound of natural *Drosophila melanogaster* courtship song. **b**, Expression patterns of the dPR1 split-Gal4 (left) and the TN1A split-Gal4 (right) in the VNC. Scale bars, 50 μm. **c**, Schematic of the paired fly optogenetic activation experiment. CsChrimson was expressed only in the male. **d–f**, Results of dPR1 stimulation. (**d**) Timings of pulse and sine song around time of the optogenetic stimulation of dPR1 in an example fly. (**e**) Time course of the proportions of pulse (red) and sine (blue) song induced by LED stimulation. Data are represented as mean ± s.e.m. across flies (n = 12 flies). **f**, The mean difference in the proportions of pulse (left) and sine (right) song between the stimulation and 5-s pre-stimulation periods. Each dot represents a fly. Lines represent mean ± s.d. across flies (n = 12 flies). **g–i**, Same as **d–f** but for TN1A (n = 11 flies).

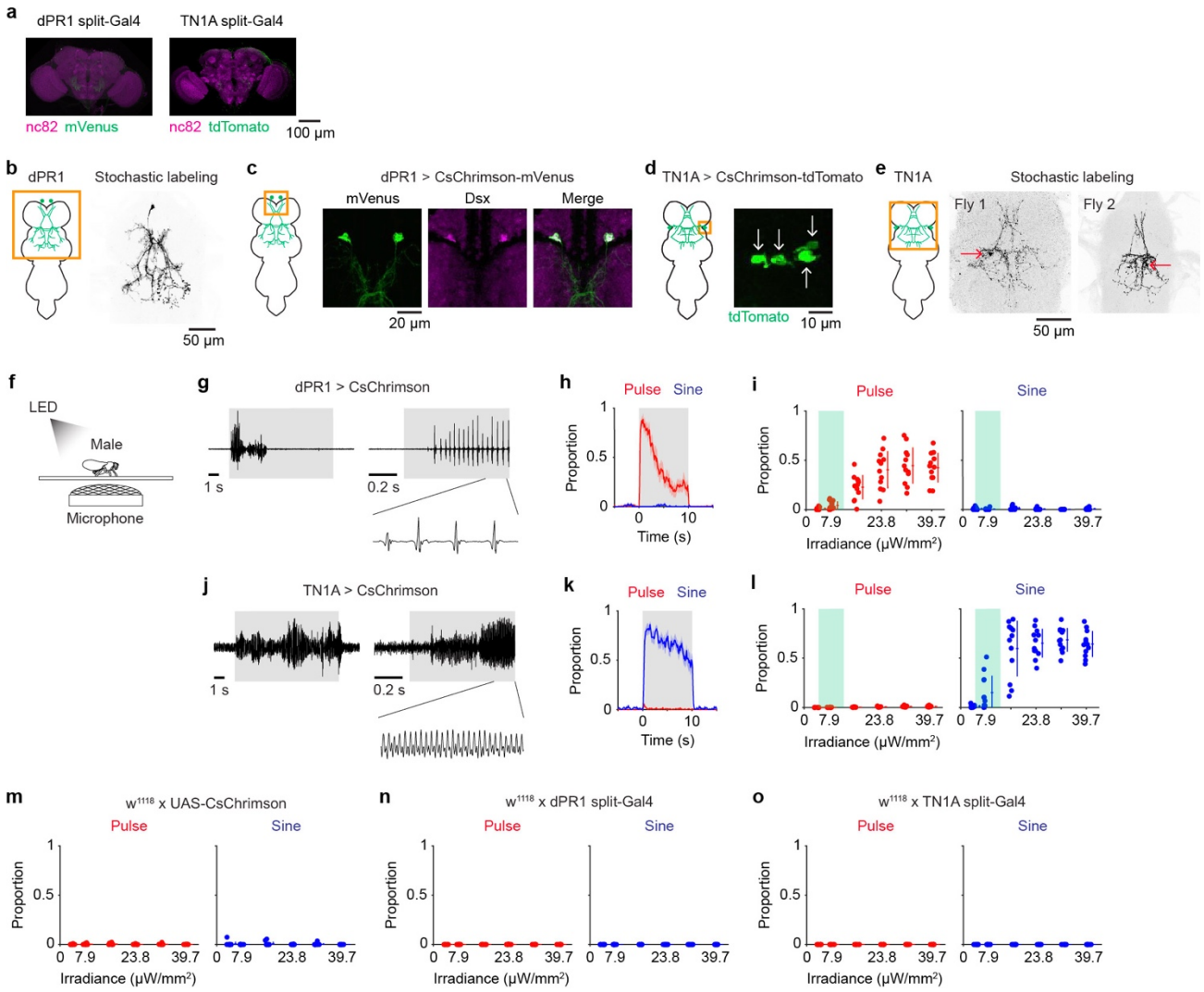

Extended Data Fig. 1 | Optogenetic activation of dPR1 and TN1A differentially induce pulse and sine song in solitary flies. a, Expression patterns of the dPR1 split-Gal4 (left) and the TN1A split-Gal4 (right) in the brain. **b**, A single neuron visualized in the VNC with stochastic labeling using the dPR1 split-Gal4 line. **c**, *Dsx* is expressed in the neurons labeled with the dPR1 split-Gal4 line. **d**, Cell body expression pattern of CsChrimson in the TN1A split-Gal4 line. Arrows indicate the location of cell bodies. **e**, Examples of single TN1A neurons visualized with stochastic labeling using the TN1A split-Gal4. Arrows indicate the cell bodies. **f**, Schematic of the single fly optogenetic activation experiment. **g**, Example of the sound induced by optogenetic activation of dPR1. The shaded area represents the period where LED stimulation was applied. **h**, Time course of the proportions of pulse (red) and sine (blue) song induced by LED stimulation at an irradiance of 15.9 µW/mm^2. Data are represented as mean ± s.e.m. across flies (n = 12 flies). **i**, The mean proportions of pulse (left) and sine (right) song during the stimulation period. Each dot represents a fly. Lines represent mean ± s.d. across flies (n = 12 flies). Shaded areas indicate the range of light intensities that were used in the paired fly optogenetic activation experiment. **j–l**, Same as **g–i** but for TN1A (n = 12 flies). **m–o**, Results for control flies in the single fly optogenetic stimulation experiment. The mean proportions of pulse and sine song during

721 the stimulation period. Each dot represents a fly. Lines represent mean ± s.d. across flies (**m,** n = 11 flies; **n**, n = 12
722 flies; **o**, n = 12 flies).

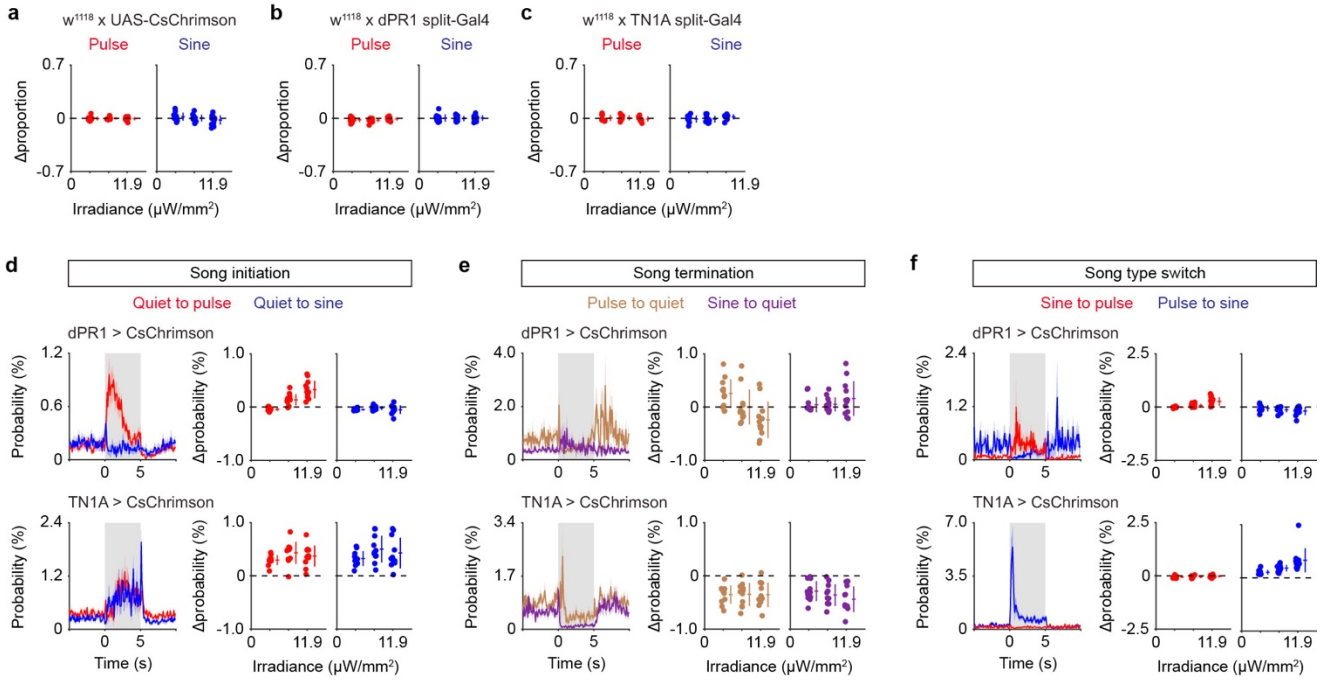

Extended Data Fig. 2 | Optogenetic activation of dPR1 and TN1A modulates pulse and sine song production in distinct ways. a–c, Results for control flies in the paired fly optogenetic stimulation experiment. The mean difference in the proportions of pulse and sine song between the stimulation and 5-s pre-stimulation periods. Each dot represents a fly. Lines represent mean ± s.d. across flies (**a,** n = 12 flies; **b**, n = 12 flies; **c**, n = 10 flies). **d–f**, Analysis of transition probabilities in the paired fly optogenetic activation experiment. Top, results of dPR1 activation (n = 12 flies). Bottom, results of TN1A activation (n = 11 flies). Left, time course of transition probabilities during LED stimulation at an irradiance of 11.9 μW/mm^2. Data are represented as mean ± s.e.m. across flies. Right, the mean difference in the transition probabilities between the stimulation and 5-s pre-stimulation periods. Each dot represents a fly. Lines represent mean ± s.d. across flies. (**d**) The probabilities of quiet to pulse (red) and quiet to sine (blue) transitions. (**e**) The probabilities of pulse to quiet (brown) and sine to quiet (purple) transitions. (**f**) The probabilities of sine to pulse (red) and pulse to sine (blue) transitions.

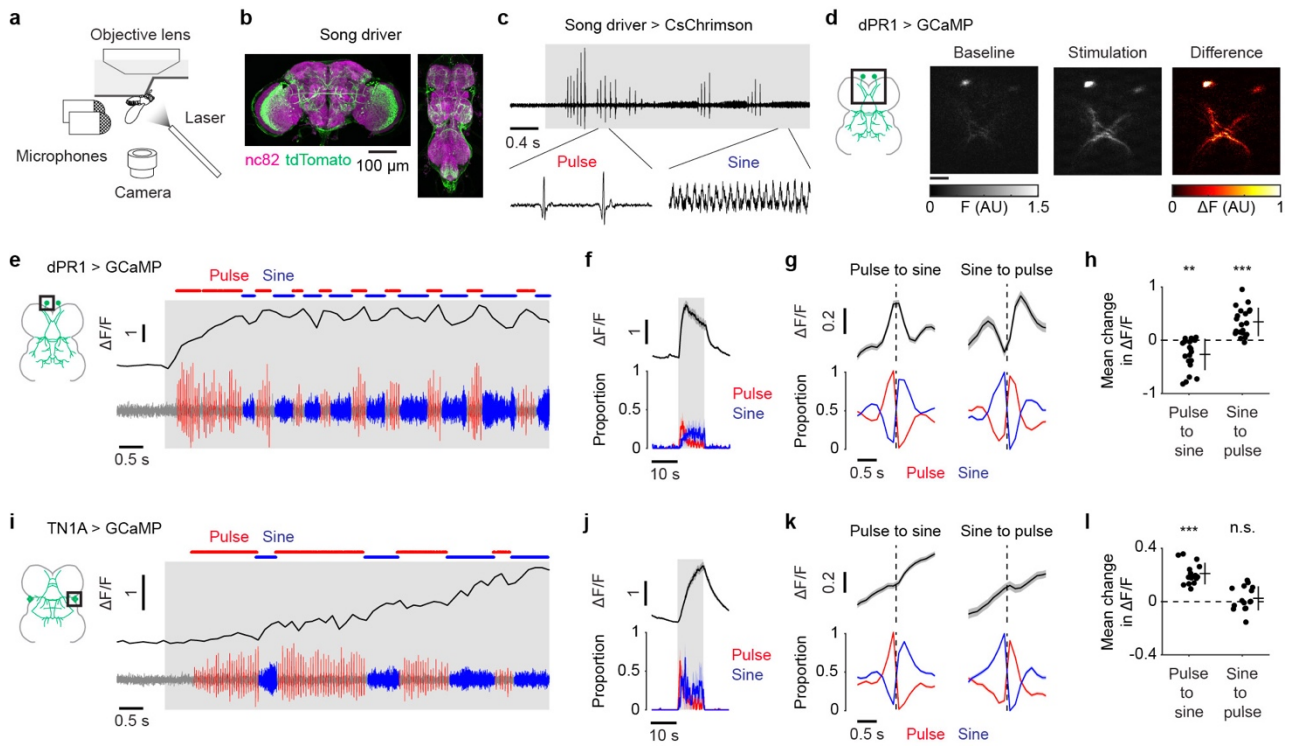

Fig. 2 | dPR1 and TN1A exhibit distinct activity patterns during song. a, Schematic of calcium imaging during fly singing. **b**, Expression pattern of the driver line used to induce pulse and sine song with optogenetic activation. **c**, Example of the sounds induced by optogenetic activation of the song driver in a fly attached to the recording plate. No thoracic dissection was made prior to this recording. The shaded area represents the period when laser stimulation was applied. **d**, Example frames during recording from dPR1. Scale bar, 20 µm. **e**, Example ΔF/F trace of a single dPR1 neuron (top) together with the simultaneously recorded sound (bottom). **f**, Time course of ΔF/F recorded from dPR1 (top) and the proportions of pulse and sine song (bottom) during laser stimulation at an irradiance of 9.8 $\mu W/mm^2$. Data are represented as mean ± s.e.m. across neurons (top; n = 18 neurons in 9 flies) and flies (bottom; n = 9 files). **g**, Time course of dPR1 ΔF/F (top) and song (bottom) around song-type transitions. Dashed vertical lines represent the timing of transitions. Data are from 20 neurons in 10 flies and represented as mean ± s.e.m. across transitions for both ΔF/F and song (n = 2184 and 858 events for pulse-to-sine and sine-to-pulse transitions, respectively). **h**, The mean change in ΔF/F after song-type transitions (see Methods for detail) for dPR1. Each dot represents a neuron. Lines represent mean ± s.d. across neurons (n = 20 neurons in 10 flies). **$P < 0.01/2$, ***$P < 0.001/2$, one-sample t test with Bonferroni correction, the denominator represents the number of comparisons. **i–l**, Same as **e–h** but for TN1A. (**j**) n = 15 neurons in 4 flies. (**k**) n = 967 (pulse-to-sine) and 444 (sine-to-pulse) transitions from 15 neurons in 4 flies. (**l**) n = 15 neurons in 4 flies.

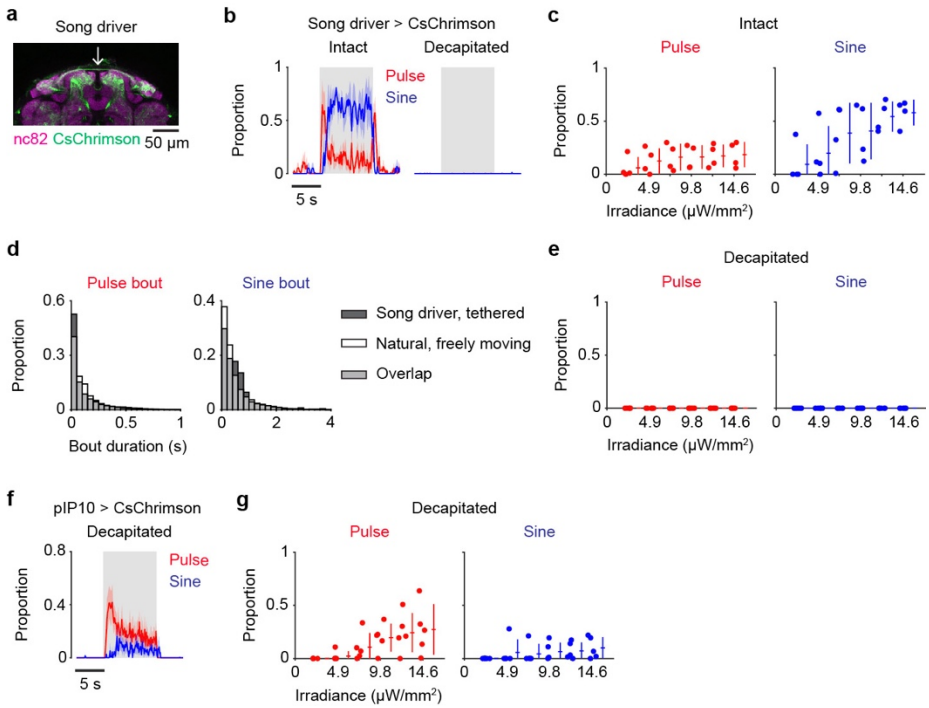

Extended Data Fig. 3 | Characterization of the song driver R22D03-LexA. a, Expression pattern of the song driver at an anterior-dorsal part of the central brain of a male fly. The arrow indicates the commissural fibers of P1 neurons. **b**, Flies expressing CsChrimson under the control of the song driver were attached to the recording plate and optogenetically stimulated with a red laser. For the decapitated group, the head was removed after attachment to the recording plate. No thoracic dissection was made on these flies. The graphs show the time course of the proportions of pulse and sine song during laser stimulation at an irradiance of 12.2 μW/mm^2. Data are represented as mean ± s.e.m. across flies (n = 4 flies for the intact group; n = 6 flies for the decapitated group). **c**, The mean proportions of pulse (left) and sine (right) song during the stimulation period for the intact group. Each dot represents a fly. Lines represent mean ± s.d. across flies (n = 4 flies). **d**, The distributions of the durations of pulse and sine song bouts. Dark grey bars, the songs induced by optogenetic activation with the song driver (n = 4 intact flies). White bars, the songs in a group of control flies in the paired fly optogenetic stimulation experiment shown in Extended Data Fig. 2a (w^{1118} crossed to UAS-CsChrimson; n = 12 flies). **e**, Same as **c** but for the decapitated group (n = 6 flies). **f**, Flies expressing CsChrimson under the control of the split-Gal4 line for pIP10 were attached to the recording plate, decapitated and provided with optogenetic stimulation. No dissection was made on the thorax. Graphs show time courses of the proportions of pulse and sine song during laser stimulation at an irradiance of 12.2 μW/mm^2. Data are represented as mean ± s.e.m. across flies (n = 5 flies). **g**, Same as **e** but for pIP10 (n = 5 flies).

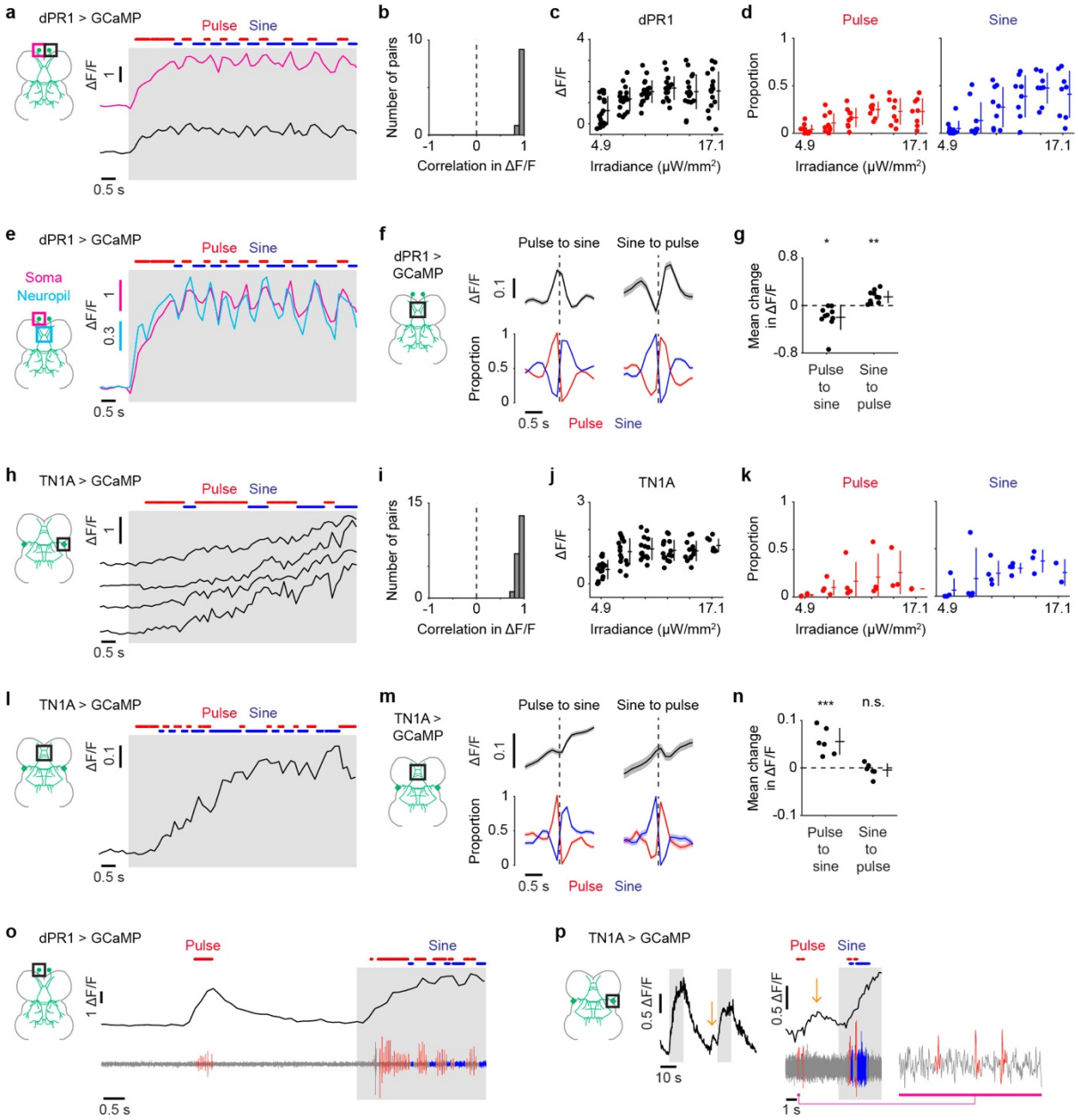

Extended Data Fig. 4 | dPR1 and TN1A exhibit distinct activity patterns during song. a, Example ΔF/F traces of two dPR1 neurons recorded simultaneously. The top trace is the same as the one shown in Fig. 2**e**. The song driver was used to express CsChrimson. The shaded area represents the period where laser stimulation was applied. **b**, Histogram of the Pearson's correlation coefficients between pairs of dPR1 neurons recorded simultaneously (n = 10 pairs in 10 flies). **c**, The mean ΔF/F during the stimulation period for dPR1. Each dot represents a neuron. Lines represent mean ± s.d. across neurons (n = 16–20 neurons in 8–10 flies for each irradiance). **d**, The mean proportions of pulse and sine song during the stimulation period in the recordings from dPR1. Each dot represents a fly. Lines represent mean ± s.d. across flies (n = 8–10 flies for each irradiance). **e**, Example ΔF/F trace of a part of the dPR1 neurite (cyan) along with that of a cell body recorded simultaneously (magenta). The trace for the cell body is the same as the one shown in Fig.

2**e**. **f**, Time course of dPR1 neurite ΔF/F and song around song-type transitions. Dashed vertical lines represent the transition times. Data are from 10 flies and represented as mean ± s.e.m. across transitions for both ΔF/F and song (n = 1092 and 429 events for pulse-to-sine and sine-to-pulse transitions, respectively). **g**, The mean change in ΔF/F after song-type transitions for the neurite of dPR1. Each dot represents a fly. Lines represent mean ± s.d. across flies (n = 10 flies). *P < 0.05/2, **P < 0.01/2, one-sample t test with Bonferroni correction, the denominator represents the number of comparisons. **h**, Example ΔF/F traces of four TN1A neurons recorded simultaneously. The top trace is the same as the one shown in Fig. 2**i**. **i**, Histogram of the Pearson's correlation coefficients between pairs of TN1A neurons recorded simultaneously (n = 21 pairs in 4 flies). **j**, Same as **c** but for TN1A (n = 8–15 neurons in 2–4 flies). **k**, Same as **d** but for the recording from TN1A (n = 2–4 flies for each irradiance). **l**, Example ΔF/F trace of a part of the TN1A neurite. **m**,**n**, Same as **f** and **g** but for TN1A. (**m**) n = 318 pulse-to-sine and 122 sine-to-pulse transitions in 6 flies. (**n**) n = 6 flies. **o**, Example ΔF/F trace of a single dPR1 neuron (top) together with the simultaneously recorded sound (bottom). The fly produced a train of pulse song outside the stimulation period, which was accompanied by an increase in calcium signals. **p**, Example ΔF/F trace of a single TN1A neuron. The fly produced pulse song outside the stimulation period, which was followed by an increase in calcium signals (arrows).

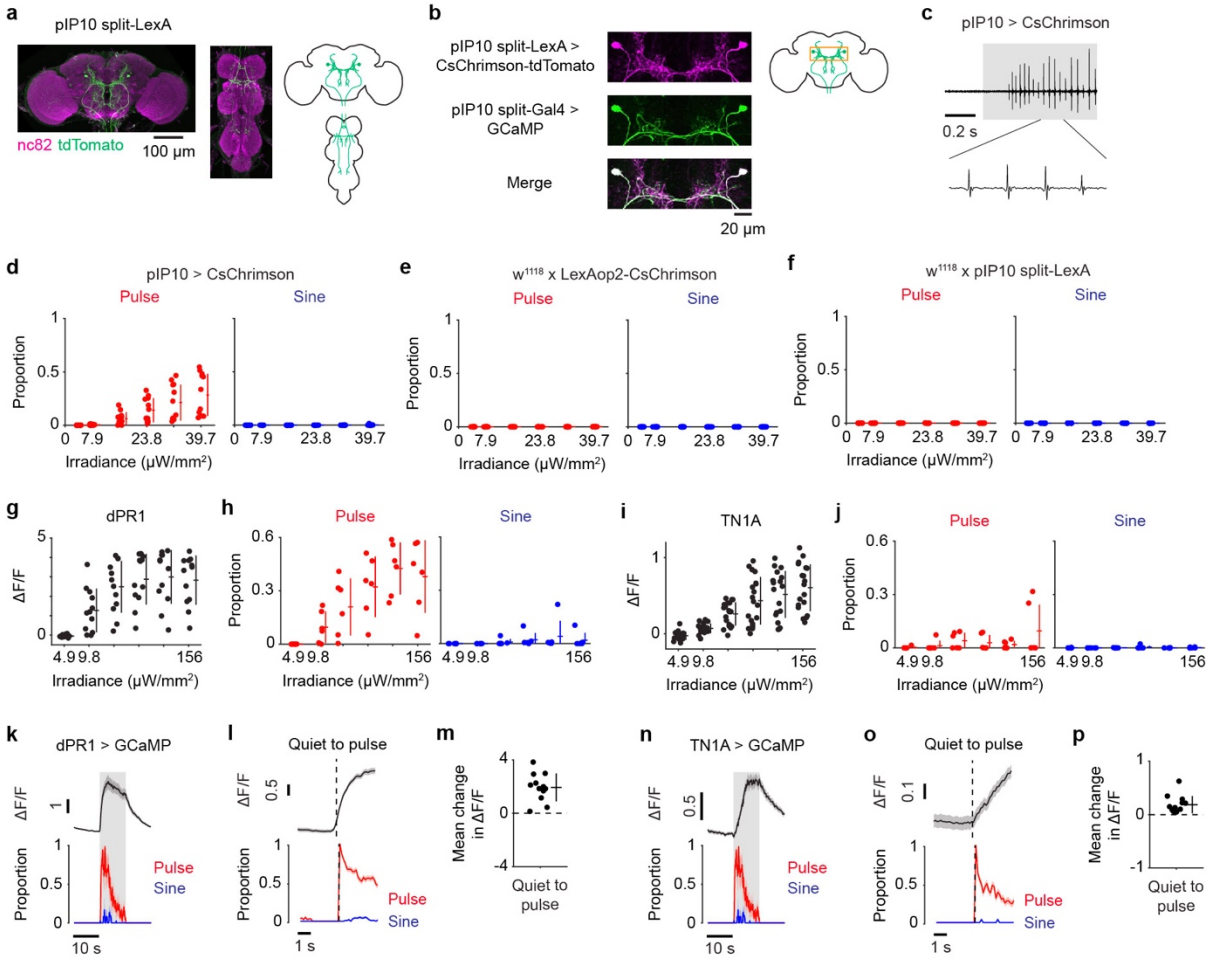

Extended Data Fig. 5 | dPR1 and TN1A are activated during pulse song induced by stimulation of the descending neurons pIP10. a, Expression pattern of the split-LexA driver for pIP10. **b**, Expression patterns of the pIP10 split-LexA and split-Gal4 drivers around the cell bodies of pIP10. **c**, Example of the sound induced by optogenetic activation of pIP10 in the single fly optogenetic activation experiment. The shaded area represents the period of LED stimulation. **d**, The mean proportions of pulse and sine song during the stimulation period in the single fly optogenetic activation experiment. Each dot represents a fly. Lines represent mean ± s.d. across flies (n = 12 flies). **e**,**f** Same as **d** but for control flies. (**e**) n = 12 flies. (**f**) n = 12 flies. **g**, The mean ΔF/F of dPR1 during the stimulation of pIP10. jGCaMP7s was expressed with *dsx*-Gal4 and calcium signals were recorded from dPR1 cell bodies. Each dot represents a neuron. Lines represent mean ± s.d. across neurons (n = 12 neurons in 6 flies). **h**, The mean proportions of pulse and sine song during the stimulation period in the recordings from dPR1. Each dot represents a fly. Lines represent mean ± s.d. across flies (n = 6 flies). **i**,**j**, Same as **g** and **h** but for TN1A. (**i**) n = 19 neurons in 6 flies. (**j**) n = 6 flies. **k**, Time course of ΔF/F recorded from dPR1 and the proportions of song for the laser stimulation at the irradiance of 156.2 µW/mm^2. Data are represented as mean ± s.e.m. across neurons (top; n = 12 neurons in 6 flies) and flies (bottom; n = 6 files). **l**, Time course of dPR1 ΔF/F and song around transitions from quiet to pulse song production. Dashed vertical lines represent the transition time. Data are from 12 neurons in 6 flies and represented as mean ± s.e.m. across transitions for both ΔF/F and song (n = 190 transitions). **m**, The mean change in ΔF/F after quiet-to-pulse transitions (see Methods for

810 detail) for dPR1. Each dot represents a neuron. Lines represent mean ± s.d. across neurons (n = 12 neurons in 6 flies).

811 **n–p**, Same as **k-m** but for TN1A. GCaMP was expressed with the TN1A split-Gal4 line. (**k**) n = 19 neurons in 6 flies.

812 (**l**) n = 99 transitions from 13 neurons in 4 flies. (**m**) n = 13 neurons in 4 flies.

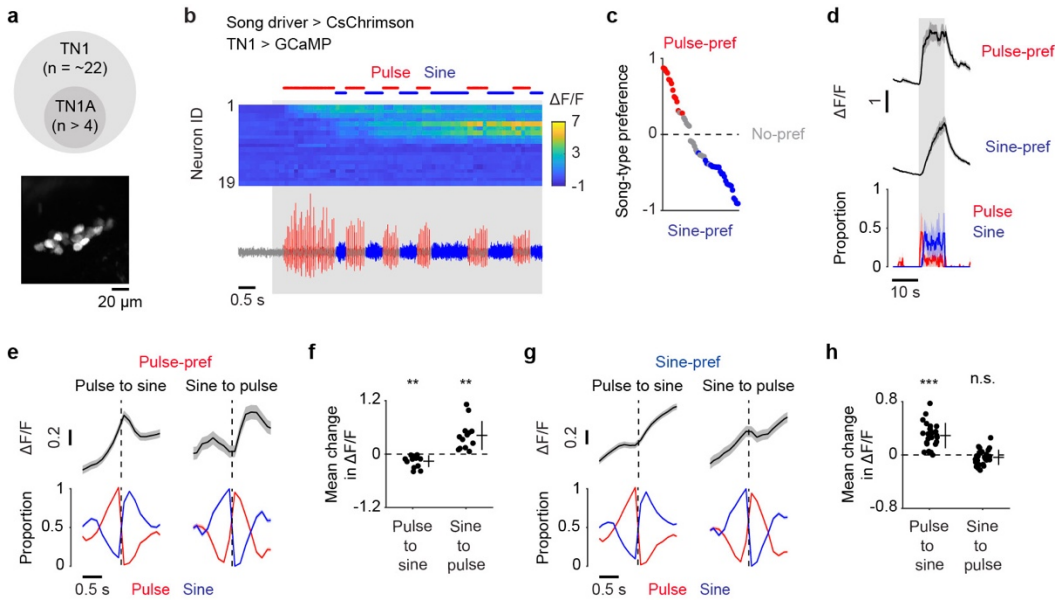

Fig. 3 | TN1 neurons with opposite song preferences exhibit different activity patterns during song. a, Top, there are approximately twenty two TN1 neurons in each hemisphere of the VNC[36]. TN1A neurons are a subset of all TN1 neurons. Bottom, example calcium signals from TN1 neurons in one hemisphere *in vivo*. GCaMP was driven by *dsx*-Gal4. The image is a maximum projection of a stack of 10 z-planes. **b**, Example ΔF/F of a population of TN1 cell bodies recorded simultaneously in a single individual (top) together with the sound recording (bottom). The song driver was used to express CsChrimson. The shaded area represents the period where laser stimulation was applied. **c**, The distribution of the song-type preference (n = 56 neurons in 4 flies), which quantifies how much calcium signals differed between pulse and sine song around song-type transitions (see Methods for detail). Red and blue dots indicate neurons whose calcium signals were significantly higher for pulse and sine, respectively ($p < 0.05$, permutation test). **d**, Time course of ΔF/F recorded from pulse-preferring and sine-preferring TN1 neurons (top) and the proportions of pulse and sine song (bottom) for the laser stimulation at an irradiance of 9.8 $\mu W/mm^2$. Data are represented as mean ± s.e.m. across neurons (top; n = 13 pulse-preferring in 3 flies and 25 sine-preferring neurons in 4 flies) and flies (bottom; n = 4 files). **e**, Time course of ΔF/F of pulse-preferring TN1 neurons (top) and song (bottom) around song-type transitions. Dashed vertical lines represent the transition time. Data are from 13 neurons in 3 flies and represented as mean ± s.e.m. across transitions for both ΔF/F and song (n = 825 and 315 events for pulse-to-sine and sine-to-pulse transitions, respectively). **f**, The mean change in ΔF/F after song-type transitions (see Methods for detail) for pulse-preferring TN1 neurons. Each dot represents a neuron. Lines represent mean ± s.d. across neurons (n = 13 neurons in 3 flies). **g**,**h**, Same as **e** and **f** but for sine-preferring TN1 neurons. (**g**) n = 1370 (pulse-to-sine) and 511 (sine-to-pulse) transitions from 25 neurons in 4 flies. (**h**) n = 25 neurons in 4 flies.

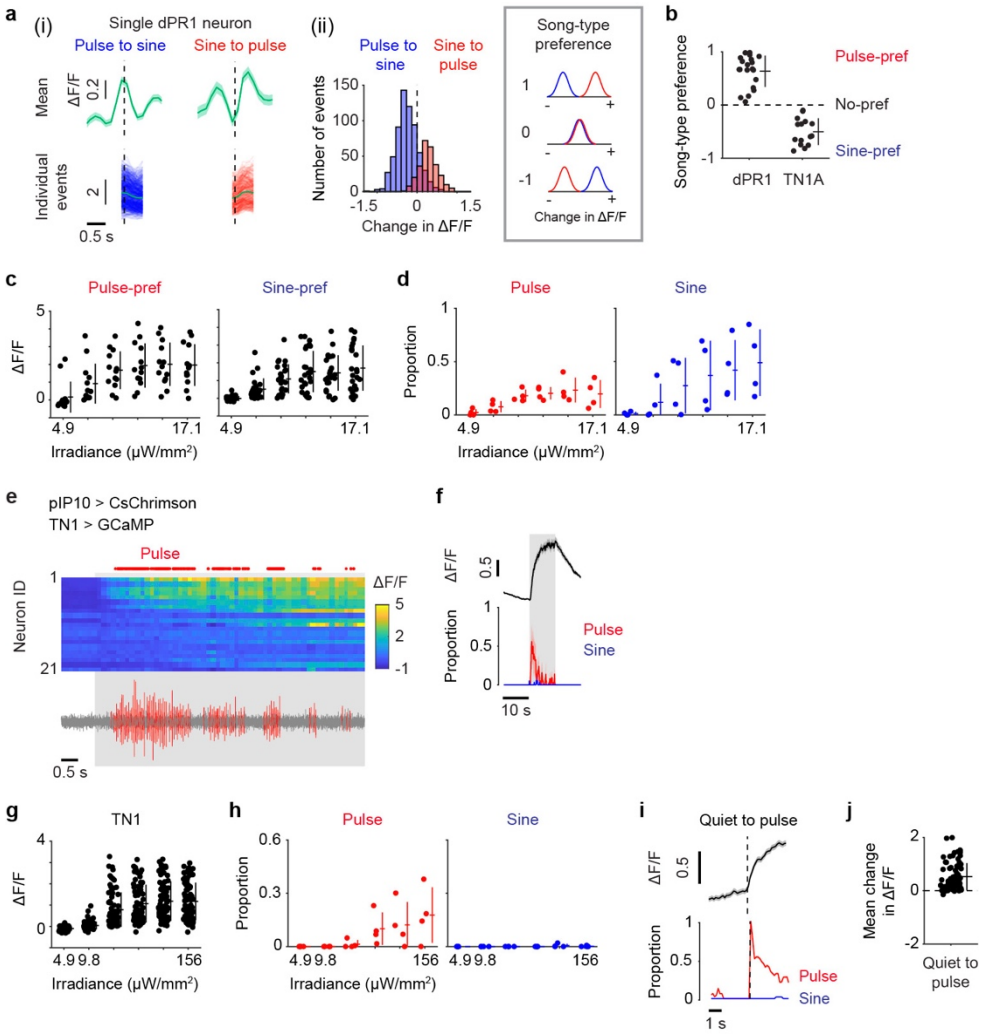

Extended Data Fig. 6 | Characterizations of TN1 responses during song production. a, Calculation of the song-type preference for an example dPR1 neuron. This index quantifies the selectivity for pulse and sine song during song-type transitions for individual neurons and is calculated in two steps (see Methods for detail). (i) First, the time course of ΔF/F around the transition is calculated for pulse-to-sine and sine-to-pulse transitions. As an example, the mean ΔF/F across events (top) and individual ΔF/F traces for each event (bottom) around song-type transitions are shown for one dPR1 neuron. Dashed vertical lines represent the transition time. For individual traces, only the part of the data used in the calculation of the index is shown. (ii) Second, histograms are calculated for the change in ΔF/F around the song-type transitions for pulse-to-sine (blue) and sine-to-pulse (red) transitions and the song-type preference is calculated using the receiver operating characteristics analysis. The song-type preference for this example dPR1 neuron was 0.87. **b**, Histograms for the song-type preference for dPR1 (n = 20 neurons in 10 flies) and TN1A (n = 15 neurons in 4 flies) calculated using the data shown in Fig. 2. **c**, The mean ΔF/F for pulse-preferring and sine-preferring TN1 neurons during the stimulation of the neurons labeled by the song driver. Each dot represents a neuron. Lines represent mean ± s.d. across neurons (n = 13 pulse-preferring and 25 sine-preferring neurons in 4 flies for each irradiance). **d**, The mean proportions of pulse and sine song during the stimulation period for the data shown in **c** (n = 2–4 flies for

848 each irradiance). Each dot represents a fly. **e–j**, Calcium imaging from TN1 cell bodies during simulation of pIP10.
849 CsChrimson was expressed using the pIP10 split-LexA driver. (**e**) Example ΔF/F of a population of TN1 neurons
850 recorded simultaneously (top) together with the sound recording (bottom). The shaded area represents the period where
851 laser stimulation was applied. (**f**) Top, Time course of ΔF/F for the TN1 neurons that showed significant responses to
852 optogenetic stimulation ($p < 0.05$, t-test; n = 77 neurons in 4 flies) for the laser stimulation at the irradiance of 78.1
853 $\mu W/mm^2$. Bottom, The proportions of song during the recording from these neurons. Data are represented as mean ±
854 s.e.m. across neurons (top) and flies (bottom). (**g**) The mean ΔF/F for pulse-preferring and sine-preferring TN1 neurons
855 during stimulation of pIP10. Each dot represents a neuron. Lines represent mean ± s.d. across neurons (n = 77 neurons
856 in 4 flies). (**h**) The mean proportions of pulse and sine song during the stimulation period for the data shown in **g** (n = 4
857 flies). Each dot represents a fly. (**i**) Time course of TN1 ΔF/F and song around transitions from quiet to pulse song
858 production. Dashed vertical lines represent the transition times. Data are from 77 neurons in 4 flies and represented as
859 mean ± s.e.m. across transitions for both ΔF/F and song (n = 869 transitions). (**j**) The mean change in ΔF/F after quiet-
860 to-pulse transitions (see Methods for detail) for TN1. Each dot represents a neuron. Lines represent mean ± s.d. across
861 neurons (n = 77 neurons in 4 flies).

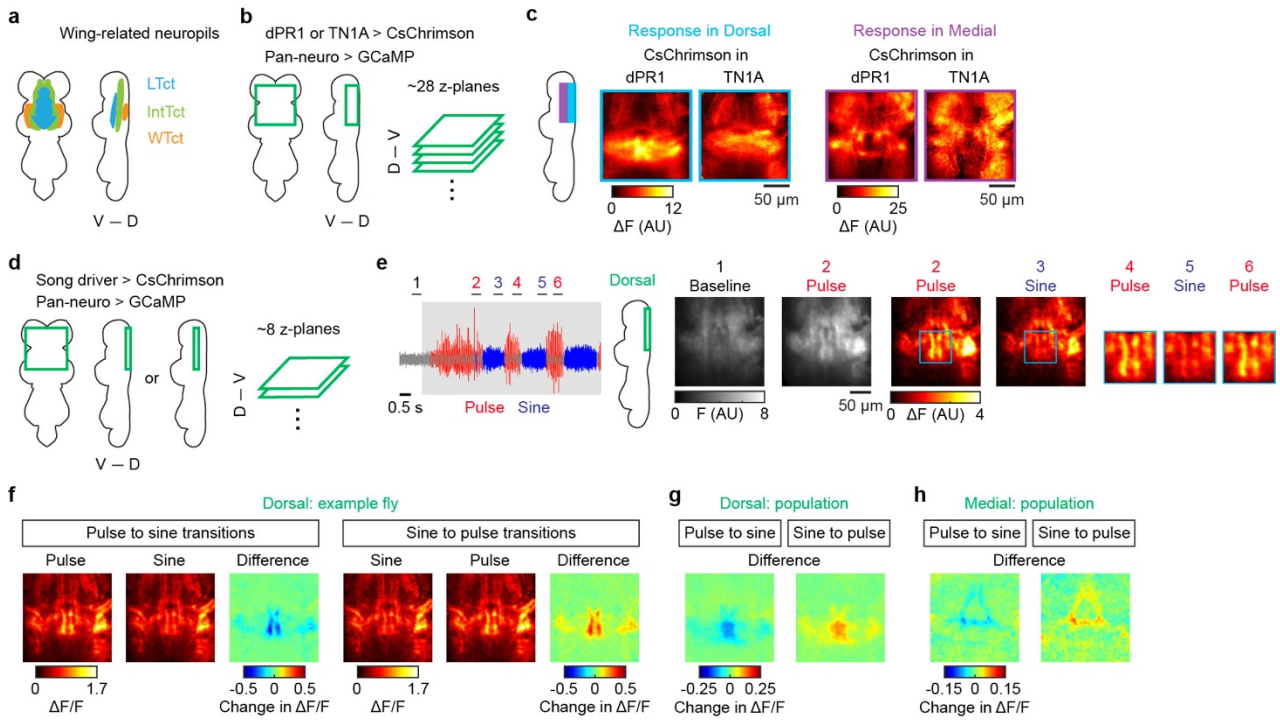

Fig. 4 | Sine song involves activation of a subset of neurons active during pulse song. a, Schematic of the wing-related neuropils. LTct, lower tectulum. IntTct, intermediate tectulum. WTct, wing tectulum. D, dorsal; V, ventral. **b**, Schematic of the VNC region imaged. GCaMP was expressed using a pan-neuronal driver. **c**, Pan-neuronal calcium imaging of the wing-related neuropils while activating either dPR1 or TN1A. Frames were averaged across trials and flies (n = 6 trials for each irradiance; n = 7 flies for dPR1, n = 6 flies for TN1A), followed by further averaging across z-planes separately for dorsal and medial volumes of the VNC. **d**, Schematic of the region imaged. For each fly, images were obtained from either a dorsal or medial part of the VNC. CsChrimson and GCaMP were expressed using the song and pan-neuronal drivers, respectively. **e**, Left, The sound data from an example recording. Bars at the top indicate periods during which example calcium imaging frames, shown on the right, are presented. The shaded area represents the period during which laser stimulation was applied. Right, Example frames. For each period, images were averaged across z-planes and time. For periods 4–6, only part of the images (blue boxes in periods 2 and 3) is shown. **f**, Changes in calcium signals around song-type transitions for an example fly where the recording was from the dorsal part of the VNC. Left, average frames during pulse to sine transitions (n = 71 transitions). Images were averaged across z-planes and time. Right, average frames during sine to pulse transitions (n = 29 transitions). **g**, Population averaged changes in ΔF/F during song-type transitions for the recordings from the dorsal part of the VNC (n = 9 flies). **h**, Same as **g** but for the recordings from the medial part (n = 3 flies).

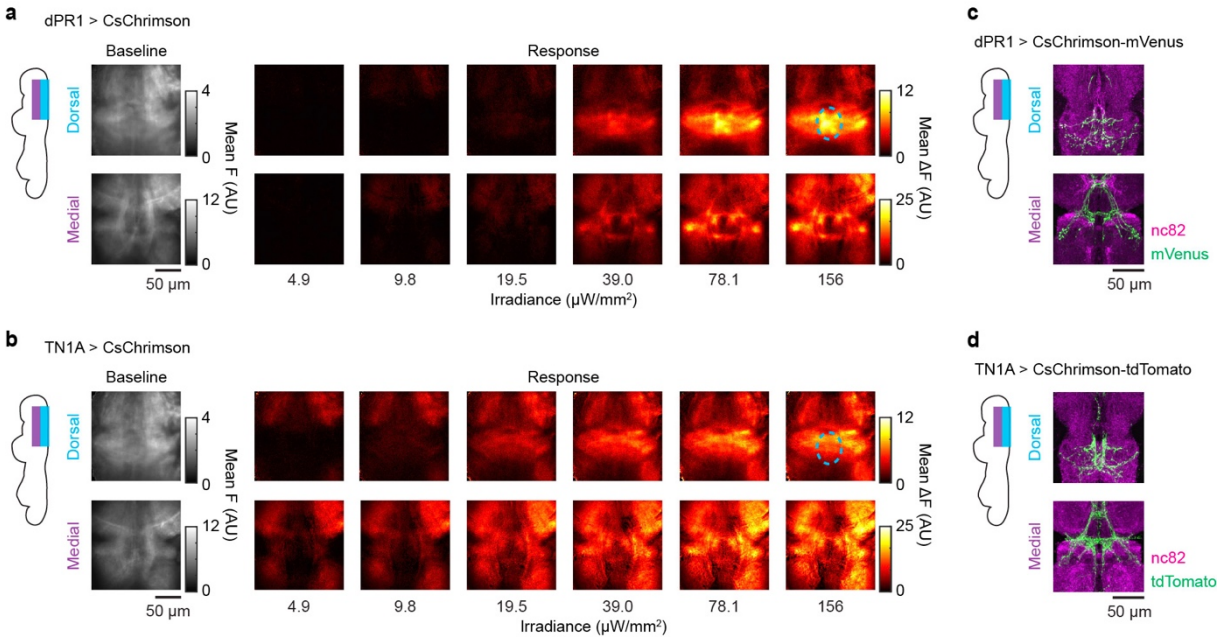

Extended Data Fig. 7 | Optogenetic stimulation of dPR1 and TN1A induce overlapping yet distinct activity patterns in the VNC. a, Pan-neuronal calcium imaging of the wing-related neuropils while activating dPR1. CsChrimson was expressed using the dPR1 split-Gal4 driver. Frames were averaged across trials and flies (n = 6 trials for each irradiance; n = 7 flies), followed by further averaging across z-planes separately for dorsal and medial volumes of the VNC. The dashed circle in the "Dorsal" image for the irradiance of 156 µW/mm^2 highlights a region that showed strong activation during dPR1 but not TN1A stimulation. **b**, Same as **a** but for TN1A (n = 6 trials for each irradiance; n = 6 flies). **c**, dPR1 neurons in the dorsal and medial volumes visualized with the dPR1 split-Gal4 line. **d**, Same as **c** but for TN1A neurons visualized with the TN1A split-Gal4 line.

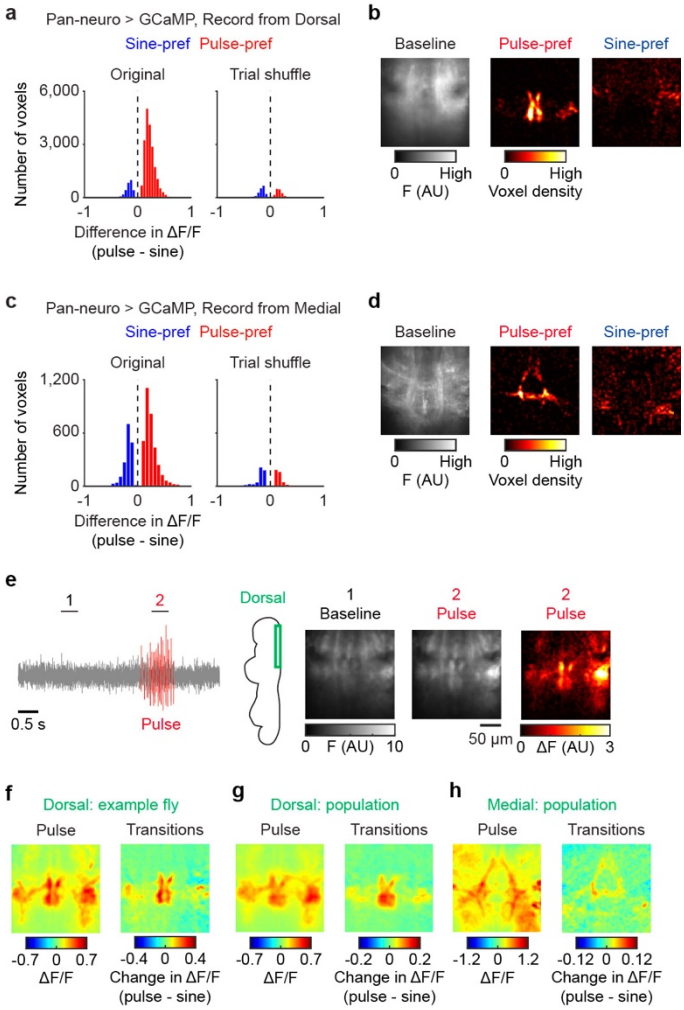

Extended Data Fig. 8 | Sine song involves activation of a subset of neurons active during pulse song. a, Histogram of the mean difference in ΔF/F between pulse and sine song during song-type transitions for the voxels which changed ΔF/F depending on song type ($p < 0.001$, permutation test). GCaMP was expressed with a pan-neuronal driver. Data of the recordings from the dorsal part of the VNC were combined (n = 22,694 voxels in 9 flies). To obtain a histogram expected by chance, the same analysis was conducted after randomizing the relationship between song and calcium signals ("Trial shuffle", see Methods). **b**, Spatial distribution of the voxels that showed higher ΔF/F during pulse ("Pulse-pref") and sine ("Sine-pref") song shown in **a**. Left, the average baseline image for the recorded volume. The image represents an average across z-planes and flies (n = 9 flies). **c**,**d**, Same as **a** and **b** but for the recordings from the medial part of the VNC. **e**, Left, The sound data for an example recording from the dorsal part of the VNC. No optogenetic stimulation was given during this 5-s recording. Bars at the top indicate periods during which example calcium imaging frames were calculated. Right, Example frames. For each period, images were averaged across z-planes and time. **f**, Left, The mean ΔF/F during the pulse song that was produced outside the optogenetic stimulation periods for the example fly shown in **e** (n = 159 frames). Right, The mean change in ΔF/F during song-type transitions for the example fly (n = 57 and 41 pulse-to-sine and sine-to-pulse transitions, respectively). Images were averaged across z-planes. **g**, Same as **f** but for the averages across flies (n = 4 flies). **h**, Same as **g** but for the recordings from the

904 medial part of the VNC (n = 2 flies).

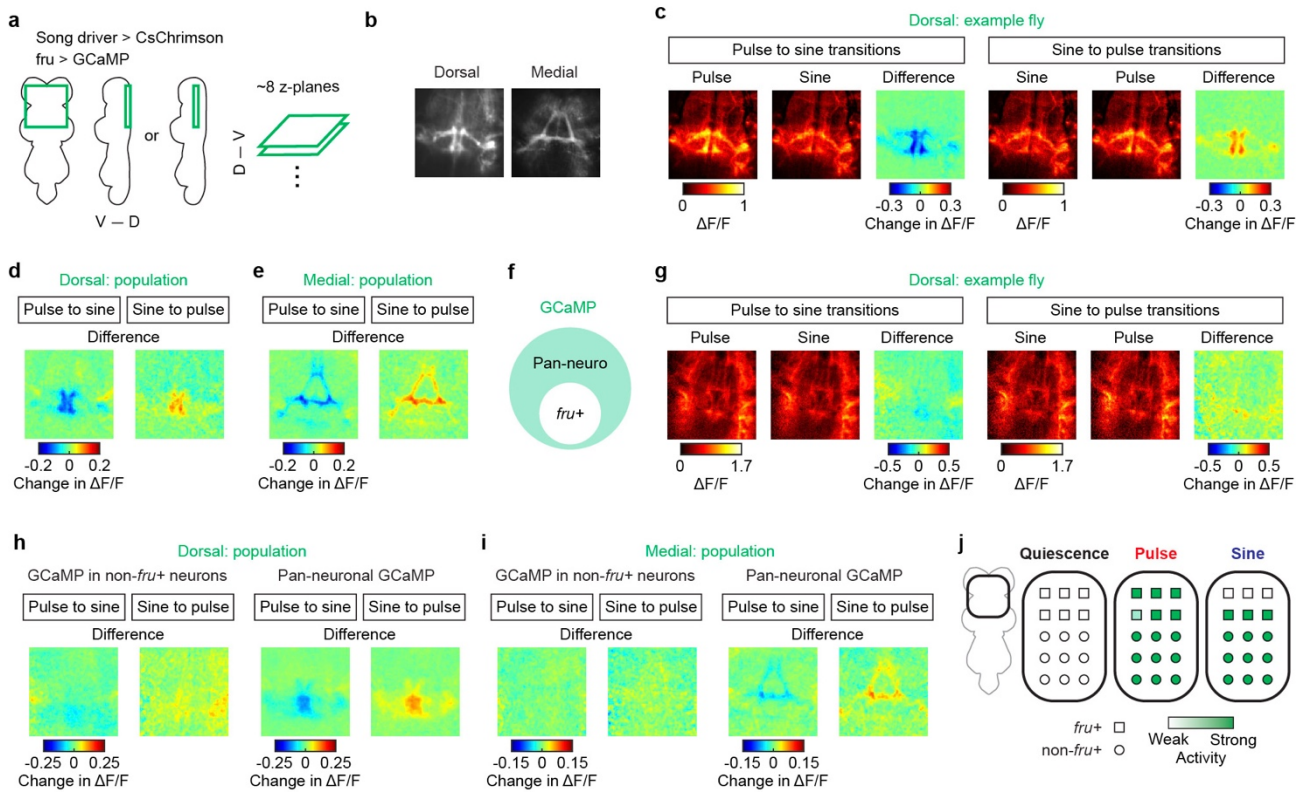

Fig. 5 | The pulse-selective neural population is mainly composed of *fru*-expressing neurons. a, Schematic of the imaged region. For each fly, images were obtained from either dorsal or medial regions of the VNC. CsChrimson and GCaMP were expressed using the song driver and *fru*-Gal4, respectively. D, dorsal; V, ventral. **b**, Example images of the calcium signals recoded from the dorsal (left) and medial (right) parts of the VNC. Images represent averages of frames across z-planes and time. **c**, Changes in calcium signals across song-type transitions for an example fly where the recording was from the dorsal part of the VNC. Left, average frames during pulse to sine transitions (n = 137 transitions). Images were averaged across z-planes and time. Right, average frames during sine to pulse transitions (n = 65 transitions). **d**, Population averaged changes in ΔF/F during song-type transitions for the recordings from the dorsal part of the VNC (n = 6 flies). **e**, Same as **d** but for the recordings from the medial part (n = 5 flies). **f–i**, Calcium imaging of non-*fru*-expressing neurons. (**f**) GCaMP was expressed using the pan-neuronal driver while its expression was suppressed in *fru*-expressing neurons. (**g**) Same as **c** but for non-*fru*-expressing neurons (n = 71 pulse to sine transitions, n = 29 sine to pulse transitions). (**h**) Population averaged changes in ΔF/F during song-type transitions for the recordings from the dorsal part of the VNC for non-*fru*-expressing neurons (Left, n = 5 flies). The pan-neuronal imaging results described in Fig. 4**g** are also shown for comparison (Right). (**i**) Same as **h** but for the recordings from the medial part (n = 3 flies). The pan-neuronal imaging results are the same as in Fig. 4**h**. (**j**) Schematic of the neural activity in the song motor circuit.

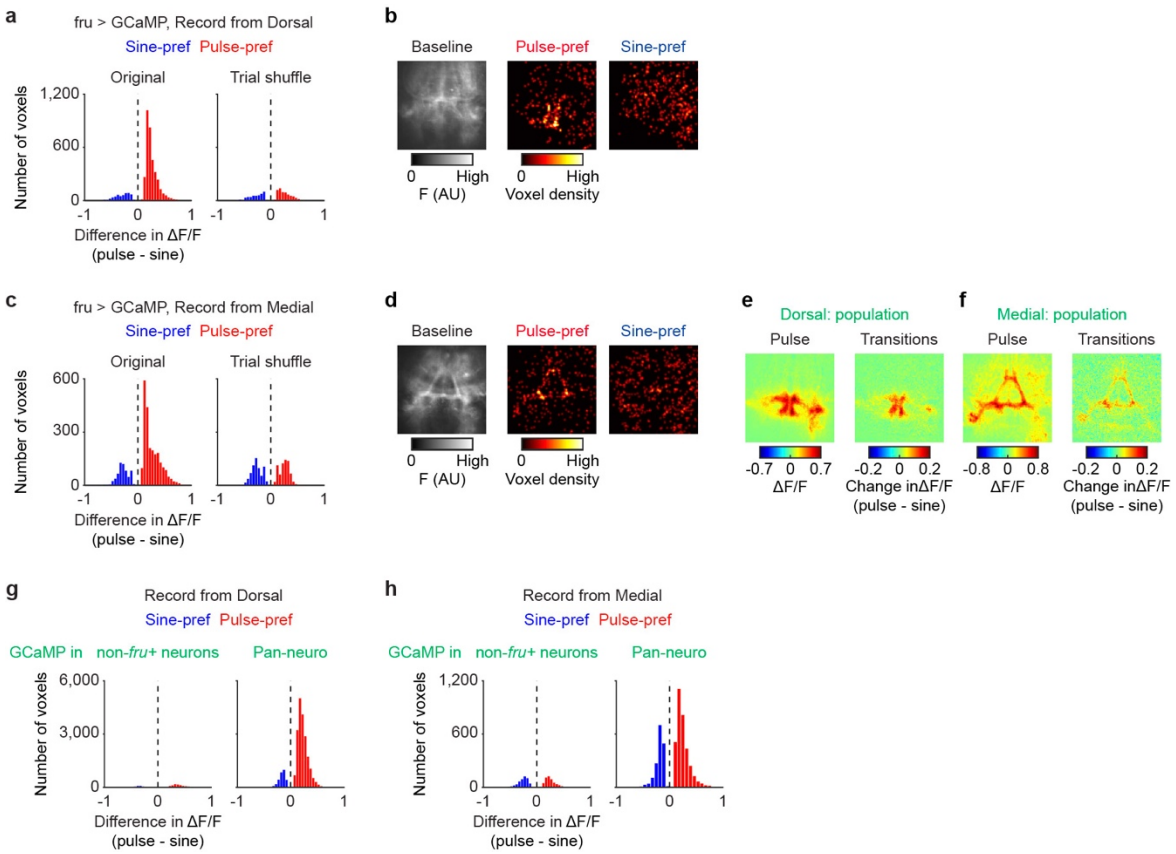

Extended Data Fig. 9 | The pulse-selective neural population is mainly composed of *fru*-expressing neurons. a, Histogram of the mean difference in ΔF/F between pulse and sine song during song-type transitions for voxels that changed ΔF/F depending on song-type ($p < 0.001$, permutation test). GCaMP was expressed with *fru*-Gal4. Data of the recordings from the dorsal part of the VNC were combined (n = 4,055 voxels in 6 flies). A histogram expected by chance was obtained using a randomization method ("Trial shuffle", see Methods). **b**, Spatial distribution of the voxels that showed higher ΔF/F during pulse ("Pulse-pref") and sine ("Sine-pref") song shown in **a**. Left, the average baseline image for the recorded volume. The image represents an average across z-planes and flies (n = 6 flies). **c**,**d**, Same as **a** and **b** but for the recordings from the medial part of the VNC (n = 5 flies). **e**, Left, The mean ΔF/F during the pulse song that was produced outside the optogenetic stimulation periods for the recordings from the dorsal part of the VNC (n = 6 flies). Right, The mean change in ΔF/F during song-type transitions (n = 6 flies). Images were averaged across z-planes. **f**, Same as f but for the recordings from the medial part of the VNC (n = 5 flies). **g**, Histograms of the mean difference in ΔF/F between pulse and sine song during song-type transitions for voxels that changed ΔF/F depending on song-type ($p < 0.001$, permutation test). Left, non-*fru*-expressing neurons (n = 1,180 voxels in 5 flies). The pan-neuronal imaging results described in Extended Data Fig. 8**a** are also shown for comparison (Right). **h**, Same as **g** but for the recordings from the medial part of the VNC (n = 1,011 voxels in 3 flies). The pan-neuronal imaging results are the same as in Extended Data Fig. 8**c**.